uOttawa

L'Université canadienne
Canada's university

FACULTÉ DES ÉTUDES SUPÉRIEURES ET POSTOCTORALES

uOttawa

L'Université canadienne
Canada's university

FACULTY OF GRADUATE AND POSDOCTORAL STUDIES

Navamshan Murugesapillai
AUTEUR DE LA THÈSE / AUTHOR OF THESIS

M.A.Sc. (Electrical Engineering)
GRADE / DEGREE

School of Information Technology and Engineering
FACULTÉ, ÉCOLE, DÉPARTEMENT / FACULTY, SCHOOL, DEPARTMENT

The Performance of the Generalized RAKE (G-RAKE) Receiver in a WCDMA-HSDPA Scenario

TITRE DE LA THÈSE / TITLE OF THESIS

A. Yongacoglu
DIRECTEUR (DIRECTRICE) DE LA THÈSE / THESIS SUPERVISOR

CO-DIRECTEUR (CO-DIRECTRICE) DE LA THÈSE / THESIS CO-SUPERVISOR

EXAMINATEURS (EXAMINATRICES) DE LA THÈSE / THESIS EXAMINERS

M. El Tanany

C. D'Amours

Gary W. Slater
LE DOYEN DE LA FACULTÉ DES ÉTUDES SUPÉRIEURES ET POSTDOCTORALES /
DEAN OF THE FACULTY OF GRADUATE AND POSTDOCORAL STUDIES

The Performance of the Generalized RAKE (G-RAKE) Receiver in a WCDMA-HSDPA Scenario

by

Navamshan Murugesapillai, B.A.Sc., P.Eng.

Thesis submitted to the
Faculty of Graduate and Postdoctoral Studies of the University of Ottawa
in partial fulfillment of the requirements for the degree of
Master of Applied Science (M.A.Sc.) in Engineering

Ottawa-Carleton Institute for Electrical and Computer Engineering
School of Information Technology and Engineering
Faculty of Engineering
University of Ottawa

Ottawa, Ontario, Canada
September 2005

Your file Votre référence
ISBN: 0-494-11360-X
Our file Notre référence
ISBN: 0-494-11360-X

Abstract

The High-Speed Downlink Packet Access (HSDPA) is a packet-based data service for increased data speed over WCDMA downlink. At high-speed data rate, advanced receivers are needed to realize a reasonable bit error performance.

This thesis studies the link-level performance of the G-RAKE receiver for the HSDPA and ways to reduce the receiver's complexity. Unlike the conventional RAKE receiver, the G-RAKE receiver suppresses interference caused by frequency-selective fading channels by accounting for coloured noise found in the fingers' output. Thus, G-RAKE optimizes the placement of fingers and the weighting coefficients in the Maximum Likelihood formulation.

In this thesis, performance of the G-RAKE is evaluated via simulations for both static and realistic multipath fading channels described in the literature. According to simulations, G-RAKE receiver compensates for the performance loss experienced by RAKE receivers when the user equipment becomes interference limited.

In G-RAKE receiver, calculating the weighting coefficients, which involves inverting the channel impairment matrix, is an expensive operation. It is shown that the complexity and processing time of this operation and, hence, of the overall receiver can be reduced with the Conjugate Gradient or Preconditioned Conjugate Gradient methods.

Table of Contents

List of Tables

List of Figures

List of Symbols

In order of use

R_{min}	Bit rate of the lowest-bit-rate-service
N_c	Chip duration
τ	Multipath delay in channel impulse response; the time difference between two samples in a random process; elapsed time
T_c	Chip period
$S_{dl,n}$	Scrambling code of length n for downlink
d	Finger delay
w	Weighting coefficient
R_b	Data rate (in bits/s)
K	Number of users/channelization codes
F_s	Sampling frequency of the RRC filter
F_d	Sampling frequency of the input data sequence
N	Spreading factor; noise power
T	Symbol duration
M	Number of constellation alphabets
h	Channel coefficient or channel impulse response
n	Noise sample
N_o	Noise power spectral density
$\mathbf{R_u}$	Channel impairment matrix or covariance matrix for a multipath fading channel
$\mathbf{u}$	Coloured noise vector
$\Lambda(.)$	log-likelihood function
$\mathbf{w}$	Vector containing weighting coefficients
$\mathbf{R_{ISI}}$	Covariance matrix due to ISI
$\mathbf{R_{MUI}}$	Covariance matrix due to MUI
$\mathbf{R_n}$	Covariance matrix due to additive noise
K	Condition number of a symmetric positive definite matrix
f_c	Carrier frequency
$P(.)$	Probability of error; Power spectral density

$R(.)$	The autocorrelation function
$\delta(.)$	Delta function
$p(.)$	The probability density function
$\mathbf{K}$	Covariance matrix for an AWGN channel
$\mathbf{n}$	Noise vector
$N(.,.)$	Normal distribution
σ^2	Variance of the noise
$\mathbf{I}$	Identity matrix
S	Input power
E_b	Average energy per information bit
E_s	Average energy per information symbol
γ_b	Instantaneous signal-to-noise ratio per bit
γ_s	Instantaneous signal-to-noise ratio per symbol
B_n	Noise bandwidth
T_{samp}	Sampling period of a signal
T_{sym}	Symbol period of a signal
α	Amplitude of the fading channel coefficient; Roll-off factor of root-raised cosine filter
$Q(.)$	Marcum Q function
Γ	Average value of the instantaneous signal-to-noise ratio
W_{ss}	Spread spectrum bandwidth
R_c	Chip Rate
W_{bb}	Baseband signal bandwidth
I_o	Total interference and noise power density at the base station
G_v	Voice activity factor for CDMA system
G_A	Antenna gain factor for CDMA system
σ_τ	Root mean square delay spread of the multipath profile
B_c	Coherence bandwidth of the fading channel
B_s	Signal bandwidth
W	Channel bandwidth
W_o	Utilized bandwidth

v	Vehicle/mobile speed
c	Speed of light
f_{max}	Maximum Doppler frequency
f_d	Doppler frequency
f_{nd}	Normalized Doppler frequency
R_{baud}	Symbol Rate

Glossary

3GPP	Third Generation Partnership Project
ADSL	Asymmetric Digital Subscriber Line
AMC	Adaptive Modulation and Coding
AWGN	Additive White Gaussian Noise
BER	Bit Error Rate
BS	Base Station
CDMA	Code Division Multiple Access
CG	Conjugate Gradient
CGN	Coloured Gaussian Noise
CQI	Channel Quality Indicator
CRC	Cyclic Redundancy Check
DCH	Dedicated channel
DPCCH	Dedicated Physical Control Channel
DPCH	Dedicated Physical Channel
DS-CDMA	Direct Sequence Code Division Multiple Access
DSP	Digital Signal Processing
ETSI	European Telecommunications Standard Institute
FDD	Frequency Division Duplexing
FDMA	Frequency Division Multiple Access
FIR	Finite Impulse Response
G-RAKE	Generalized RAKE
GS	Gauss-Seidel
H-ARQ	Hybrid-Automatic Repeat reQuest
HSDPA	High-Speed Downlink Packet Access
HS-DSCH	High-Speed Downlink Shared Channel
HS-PDSCH	High-Speed Physical Downlink Shared Channel
HS-SCCH	High-Speed Shared Control Channel
IMT-2000	International Mobile Telecommunication 2000
ISI	Inter Symbol Interference

ITU	International Telecommunications Union
LUD	LU Decomposition
MAC	Medium Access Control
MAC-hs	Medium Access Control for HSDPA
MAI	Multiple Access Interference
MCI	Multi-code Interference
MIMO	Multiple Input Multiple Output
ML	Maximum Likelihood
MRC	Maximum Ratio Combining
MS	Mobile Station
MUI	Multiple User Interference
OVSF	Orthogonal Variable Spreading Factor (codes)
PCG	Preconditioned Conjugate Gradient
PDF	Probability Density Function
PG	Processing Gain
PN	Pseudo Noise
PSD	Power Spectral Density
QAM	Quadrature Amplitude Modulation
QPSK	Quadrature Phase Shift Keying
RLC	Radio Link Control
RNC	Radio Network Controller
RR	Round robin (scheduler)
RRC	Radio Resource Control
RRC	Root-Raised Cosine
SAW	Stop and Wait
SCH	Synchronisation Channel
SF	Spreading Factor
SINR	Signal to Interference Plus Noise Ratio
SNR	Signal to Noise Ratio
SOR	Successive Over-Relaxation
SSOR	Symmetric Successive Over-Relaxation

TB	Transport Block
TCP	Transport Control Protocol
TDMA	Time Division Multiple Access
TPC	Transmit Power Control
TTI	Transmission Time Interval
WCDMA	Wideband Code Division Multiple Access
WMF	Whitening Matched Filter
UE	User Equipment
UMTS	Universal Mobile Telecommunication System
UTRAN	UMTS Terrestrial Radio Access Network

Acknowledgements

This thesis has personally shaped up my research ability and sharpened my knowledge in the exciting field of wireless communication systems. I am obliged to the following individuals without whose help and guidance this work would not have been possible.

- I am grateful to my supervisor, Prof. Abbas Yongaçoğlu, for his valuable consultations, for sharing his profound knowledge in the area of digital communication, and for his constant encouragement throughout my research. His boundless enthusiasm and guidance gave me impetus to complete this thesis.
- My special gratitude goes to Dr. Daniel Boudreau, Nortel Networks, for introducing me to the area of HSDPA, for co-supervising my work, and for suggesting interesting ideas to form the core behind my thesis. The valuable time he had spared with me whenever I approached him is always memorable.
- This work will be incomplete without expressing my appreciation to a wonderful person at the University of Ottawa. I am thankful to Mr. Tunçer Baykaş, who pursues his Ph.D, for sharing his simulation expertise, for promptly answering my e-mails with sound technical advice, and for his precious time and friendship.
- Finally, I would like to thank my father, Nagamany Murugesapillai, my mother, Alageswary Murugesapillai, my elder sister, Subajini Uthayakumaran, my younger sister, Thanujah Kugaraj, my brother, Amirthamshan Murugesapillai, my wife, Jenenthine Navamshan, my brother-in-laws, Sivapathasundaram Uthayakumaran and Pradeep Kugaraj , and my nieces, Kavina Uthayakumaran and Kaneera Uthayakumaran for their everlasting love, motivation, and influence in making me achieve this goal.

This thesis is dedicated to my Appa and Amma.

CHAPTER 1

1. Introduction

1.1 Background

The 3rd and 4th generation cellular mobile communication systems are being built to serve a variety of multimedia services in addition to voice and data. Some of these interactive services require high data rates and low bit error rate (BER). The increase in system capacity and reduced BER lead system designers to devise more advanced signal detection techniques.

Signal detection in a mobile handset is carried out in the baseband Digital Signal Processing (DSP) and requires power. Mobile handsets are powered by battery, which is a scarce source of energy. In order to maintain longer connection time (talk-time), efficient use of the transmission power is vital. In addition, consumers' desire for smaller size mobile handsets determines their evolution. Therefore, the complexity of any advanced detection technique should be kept low in a mobile receiver.

Wideband Code-Division Multiple-Access (WCDMA) is one of the main technologies for the implementation of third-generation (3G) cellular systems. It is based on radio access technique proposed by ETSI Alpha group and its specifications were first prepared in 1999 [1]. WCDMA, which is based on DS-CDMA, is also known as Universal Mobile Telecommunication Systems (UMTS) and has been adopted as a standard by the International Telecommunication Union (ITU) under the name IMT-2000. High-Speed Downlink Packet Access (HSDPA) is the evolution of WCDMA that fulfills the demand for high-speed data in the downlink (BS to MS) varying from 2-20 Mbps.

In practice, wide bandwidth signals undergo highly frequency selective fading in a time-dispersive channel due to multipath propagation and experience slow fading caused by relatively smaller Doppler spread of the channel [2]. Such fading produces high

resolution of distinct multipaths and causes multi-access-interference (MAI) and inter-symbol-interference (ISI) among transmitted signals.

Currently, low-complexity conventional RAKE receivers are used for multipath mitigation in WCDMA enabled handsets. However, the interference suppression capability of the RAKE receivers is poor as they either ignore the interference or consider it as white noise. As HSDPA gets deployed in real cellular wireless systems, it would be difficult to achieve the performance requirements for high-speed data (for example, BER of 10^{-3} as outlined in [1]) using the standard RAKE receivers in HSDPA enabled handsets as for reasons that will be explained later. Alternatively, a multistage receiver with RAKE structure can be utilized to optimize partial interference cancellation (multi-user IC) as presented in [3]. However, in practical system, it is proven that such a receiver structure requires three or four stages to achieve sound BER performance. The complexity of this structure is high and, therefore, it is not a favourable choice in a mobile handset.

A fairly complex advanced receiver termed the *Generalized* RAKE (G-RAKE) receiver is developed in [4] to optimize the performance of the conventional RAKE in the downlink. It is reported in the literature [4]-[7] that the G-RAKE gives significant improvement in capacity over the standard RAKE for WCDMA systems using QPSK modulation scheme. This thesis aims at evaluating the performance of G-RAKE receiver in the UMTS HSDPA scenario. In addition, it explores the possibility of reducing the complexity of the G-RAKE receiver.

1.2 Motivation and Thesis Contributions

As mentioned before, this study focuses on the use of G-RAKE receiver in a mobile handset for HSDPA, of which concepts and details are presented in the next chapter.

High-speed baseband processing is the main design challenge for HSDPA-enabled mobile receivers. HSDPA-enabled receivers could constitute a G-RAKE receiver to

overcome the shortcomings of a RAKE receiver. Like RAKE receiver, G-RAKE converts wide-band multipath receiver data into a narrow-band signal that is coherently combined to generate soft/hard decisions regarding the transmitted symbols at the output.

QPSK or 16-QAM modulation schemes are combined with low spreading factor codes in HSDPA to increase the data rate. However, 16-QAM provides higher spectral efficiency compared to QPSK and can thus be used to provide high peak data rates. Little can be found in the literature on the performance evaluation of G-RAKE receiver for higher-order modulation combined with low spreading factor codes. This thesis primarily studies the performance of G-RAKE receiver for 16-QAM modulation in HSDPA.

It is known that the computational complexity of a RAKE receiver linearly increases with the number of multipath components being processed. In the literature [4], it is demonstrated that the G-RAKE receiver can produce better performance when the number of fingers placed amount up to twice as many as the number of multipath components processed. Certainly, using more fingers than the number of multipaths will increase complexity. In addition, the finger delays chosen to maximize the signal-to-interference-plus-noise ratio (SINR) may or may not match the delays of the multipaths. Doing so further increases the complexity. Moreover, the combining weights are optimized based on a maximum likelihood (ML) formulation that requires additional increase in complexity. In this thesis, techniques that can be employed to reduce the complexity of the receiver are addressed.

This study is confined to link level performance analysis and complexity issues associated with the G-RAKE. Overall, this thesis contributes to the area of HSDPA by producing the performance results of G-RAKE in various channel conditions.

1.3 Thesis Outline

This thesis is organized as follows.

The 3GPP WCDMA standard is briefly described along with its evolution of HSDPA in Chapter 2.

G-RAKE is one of the advanced receiver structures proposed in the literature for use in high-speed WCDMA. Chapter 3 is devoted to presenting the full definition of the G-RAKE receiver.

One of the goals of a system designer is to reduce the complexity of the receiver without sacrificing performance. In Chapter 4, techniques that can lower the complexity of G-RAKE are explored.

A mobile receiver should operate in different channel conditions. Performance results are presented in Chapter 5 for various multipath channel environments. In addition, the performance is examined using the techniques developed in Chapter 4.

The final chapter is devoted to summarizing the analysis and suggesting future work items relevant to the area of the thesis.

CHAPTER 2

2. High Speed Data in WCDMA (UMTS)

2.1 Introduction

The Release-99 WCDMA uses a new spectrum with a 5 MHz frequency band and handles up to 2 Mbps for local area access (indoor/low-range outdoor) or 384 Kbps for wide area access (urban/suburban outdoor) [8].

To support mobile broadband services such as web browsing, video streaming, mobile gaming, and mobile music in downlink, a new UMTS packet air interface called High-Speed Downlink Packet Access (HSDPA) is developed in [9] to deliver higher data rates. HSPDA increases network capacity and supports more data users per cell than the traditional UMTS deployment. When implemented, the HSDPA framework can co-exist on the same carrier as the Release-99 WCDMA services, enabling a smooth and cost-efficient introduction of HSDPA into existing WCDMA networks. Furthermore, a user can download packet-data over HSDPA while having a speech call at the same time.

HSDPA provides download speeds that are comparable to fixed line broadband solutions (e.g. ADSL). In 3rd generation partnership project (3GPP) standards, Release-5 (phase 2) specifications focus on HSDPA to provide data rates up to approximately 10 Mbps to support packet-based multimedia services. In Release-6 (phase 3) of HSDPA, data rate of 20 Mbps with MIMO systems is presented.

High-performance User Equipment (UE) categories supporting HSDPA are introduced to realize high-speed capacity [10], each allowing different level of terminal complexity as tabulated in Table 1. Therefore, HSDPA can be considered as an upgrade to WCDMA systems offering end users significantly faster download speeds as cited "HSDPA is an add-on solution on top of 3GPP R99/R4 architecture that allows up to 3.7 Mbps peak bit rate per user for a category 6 mobile with a classical RAKE receiver, and up to 14 Mbps peak bit rate per user for a category 10 mobile with an advanced receiver" [11].

Table 1: HSDPA Capable UE Categories

UE Category	Max. No Codes	Min. Inter-TTI Interval	L1 Peak Data Rate [Mbps]	Modulation Schemes
Category 1	5	3	1.2	16QAM, QPSK
Category 2	5	3	1.2	16QAM, QPSK
Category 3	5	2	1.8	16QAM, QPSK
Category 4	5	2	1.8	16QAM, QPSK
Category 5	5	1	3.6	16QAM, QPSK
Category 6	5	1	3.6	16QAM, QPSK
Category 7	10	1	7.3	16QAM, QPSK
Category 8	10	1	7.3	16QAM, QPSK
Category 9	15	1	10.0	16QAM, QPSK
Category 10	15	1	14.0	16QAM, QPSK
Category 11	5	2	0.9	QPSK
Category 12	5	1	1.8	QPSK

The UMTS Terrestrial Radio Access Network (UTRAN), shown in Figure 1, is one of the interacting domains in a UMTS network, provides the air interface access method for UE. In this network, the Base Station is referred to as Node-B and control equipment for Base Station is called the Radio Network Controller (RNC).

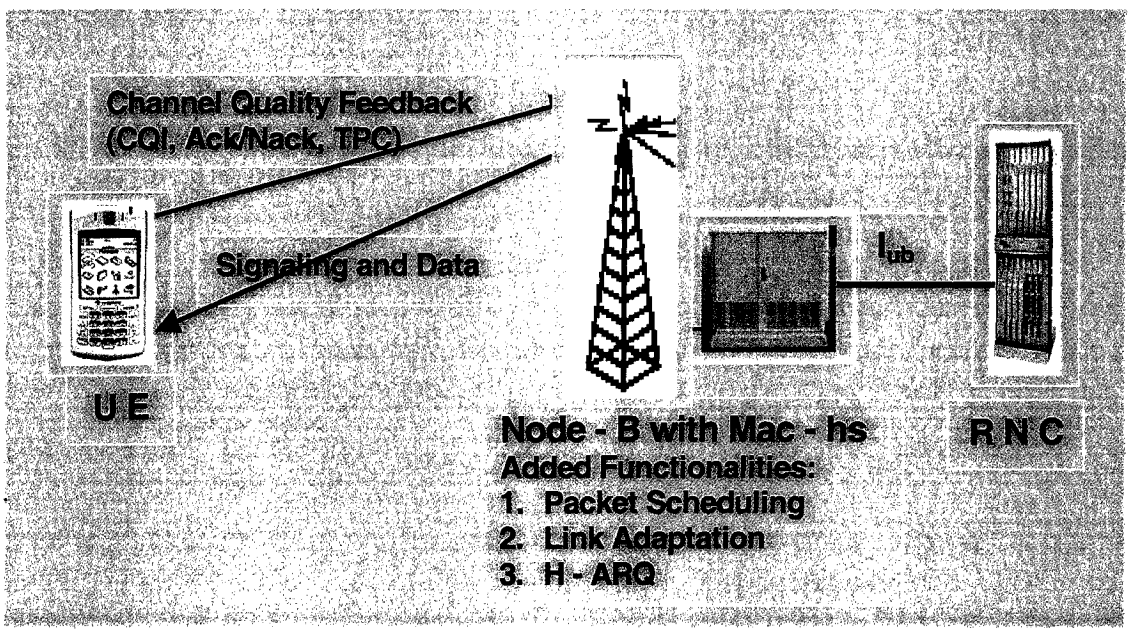

Figure 1: UMTS Terrestrial Radio Access Network with HSDPA

In HSDPA, latency of the system characterizes the quality of service for interactive applications. The delay should be reduced and the system throughput should be increased in order to provide enhanced data rates. Both are achieved by adding three fundamental technologies relying on the rapid adaptation of the transmission parameters to the instantaneous channel conditions to Node-B: fast link adaptation, fast hybrid-Automatic Repeat reQuest (H-ARQ) and fast packet scheduling [9], [13].

In subsequent sections, various components of HSDPA are briefly described.

2.2 HSDPA Channel Structure

There are three separate channel concepts (see Figure 2), through which information transfer services provided in the Frequency Division Duplexing (FDD) mode: logical, transport, and physical channels. Logical channels define the type of data transferred. Transport channels describe the characteristics (i.e. channel coding, bit rate, etc.) of the information to be sent over the radio interface. Physical channels define exact physical characteristics (i.e. channelization code, carrier frequency, etc.) of the radio link.

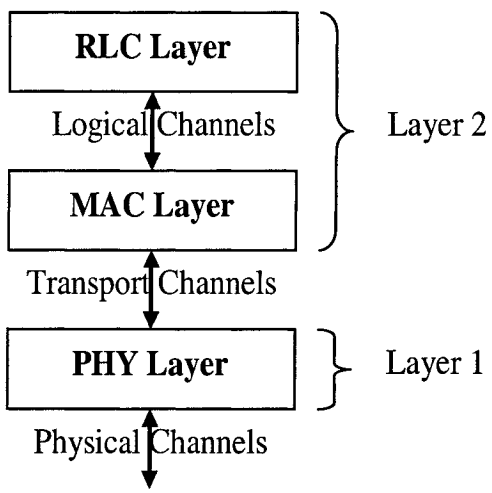

Figure 2: The Concept of Channels in WCDMA-HSDPA

As previously mentioned, HSDPA is a concept within WCDMA specifications. Its main target is to increase user peak data rates and quality of service, and to generally improve spectral efficiency for downlink asymmetrical and bursty packet data services. To enhance the peak data rate and to improve spectral efficiency over a single WCDMA carrier, a new transport channel termed High-Speed Downlink Shared Channel (HS-DSCH) is specified in [9], [13] for use by HSDPA functionality. The corresponding physical channel is denoted by HS-PDSCH as illustrated in Figure 3. The HS-DSCH shares the same carrier as other channels (i.e. DCH for voice).

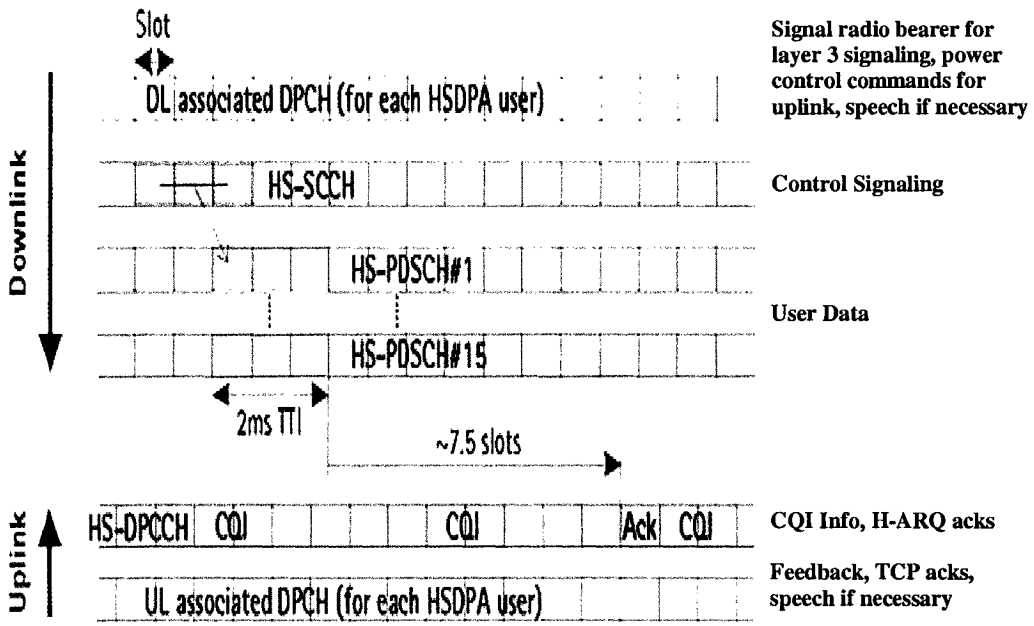

Figure 3: HS-DSCH Radio Link Structure [14]

In a standard WCDMA (Release-99) architecture, a radio frame consists of 15 timeslots and has the Transmission Time Interval (TTI) of 10 ms. Each timeslot of the radio frame has 2560 chips, resulting in a chip rate of 3.84 Mchips/s (15x2560 = 38400 chips). To reduce delays, increase the granularity in the scheduling process, and facilitate better tracking of the time-varying channel conditions, the HS-DSCH uses a substantially shorter TTI of 2 ms that is mapped to a radio sub-frame of 3 timeslots (3x2560 = 7680 chips) [11].

For HS-DSCH, the spreading factor (SF) of the modulating signal is always 16 in FDD mode [11]-[13]. The HS-DSCH code resources consist of one or more channelization codes. Up to 15 such codes can be allocated in order to leave sufficient room for other required control and data bearers. Multi-code transmission allows assignment of multiple channelization codes to a UE in the same TTI, depending on its UE capability; that is, they are allocated to one user at a time. Furthermore, multiple UEs may be assigned different subsets of the reserved channelization codes in the same TTI (i.e. multiplexing of multiple UE's in code-domain is allowed).

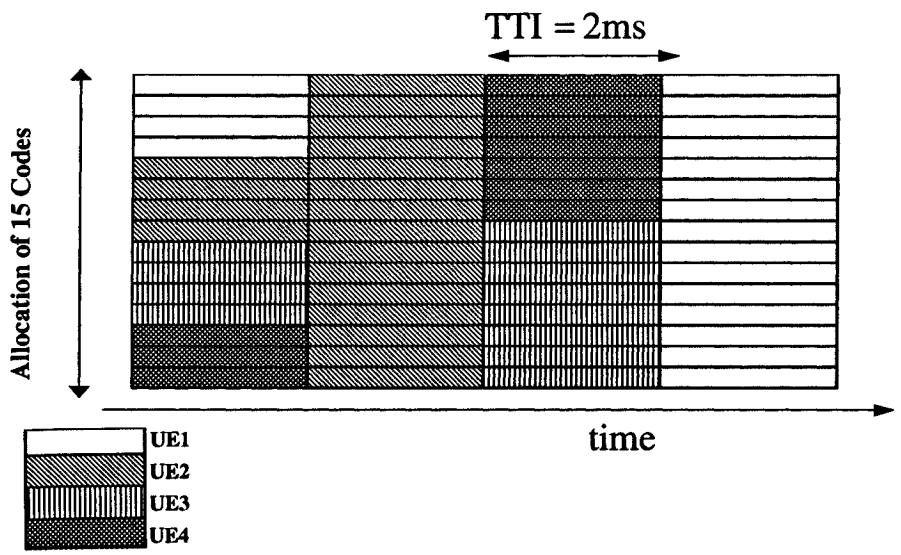

Figure 4: HS-DSCH Code Allocation Example

Figure 4 shows an example of how the reserved code resource of HS-DSCH can be allocated to up to 4 users using code multiplexing. In column 1 of the figure, from the top, the first 4 codes are allocated to UE1, the next 4 codes are allocated to UE2, the following 4 codes are allocated to UE3, and the remaining 3 codes are allocated to UE4 in a TTI. Similarly, in column 3, top 7 codes are allocated to UE4 while the remaining 8 codes in the bottom are allocated to UE3 in a TTI. On the other hand, in column 2, all 15 codes are allocated to UE2 alone. Likewise, in column 4, all 15 codes are allocated to UE1 alone. This dynamic allocation is carried out by the Node-B every TTI. For UEs

that cannot despread the full set of codes or for supporting smaller payloads, sharing the codes in code domain as shown in columns 1 and 3 is beneficial.

Besides the user data, the Node-B must also transmit control signaling to notify the next UE to be scheduled. This signaling is conducted on the physical channel called High-Speed Shared Control Channel (HS-SCCH), which is common to all users. As illustrated in Figure 3, the transmission of HS-SCCH TTI occurs two timeslots in advance of the corresponding HS-DSCH TTI. The HS-SCCH is encoded by a UE-specific mask and contains lower layer control information, including the employed settings for modulation, coding scheme, channelization code, and H-ARQ.

On top of this, each UE has an associated low bit-rate Dedicated Physical Channel (DPCH) in both the uplink and downlink directions. The downlink associated channel carries the signal radio bearer for Layer-3 signaling as well as power control commands for the uplink channel, whereas the uplink channel is used as feedback channel, carrying, for instance, the TCP acknowledgements. If needed, other services such as speech can be carried on the DPCH as well.

The HSDPA concept also introduces an additional High-Speed Dedicated Physical Control Channel (HS-DPCCH) in the uplink for carrying the Channel Quality Indicator (CQI) information as well as the H-ARQ acknowledgements. While connected, an HSDPA UE periodically sends a CQI to the Node-B indicating the data rate (as well as coding, modulation schemes, and number of multi-codes) the UE can support under its current radio conditions.

The UE also sends an acknowledgement (Ack/Nack) for each packet so that the Node-B knows when to initiate retransmissions. With the channel quality measurements available for each UE in the cell, the packet scheduler may optimize its scheduling among the users. In essence, the channel scheduler bases its selection on the highest available channel quality.

2.2.1 Adaptive Modulation and Coding (AMC) and Multi-code Transmission

The received signal strength varies over time due to fading and the geographic location of the UE in cellular communication systems (see the Appendix section A.5 for details). As a result, the variation of the signal to interference plus noise ratio (SINR) of the received signal typically ranges from 30-40 dB in the absence of power control. In order to improve system capacity, peak data rate, and coverage reliability, the signal transmitted to a particular user is modified to account for the signal quality variation through a process referred to as link adaptation.

UEs that are either stationary, relatively close to Node-B, impacted little by multipath fading and shadowing effects, or experiencing minimal other cell interference do not need to transmit with the same power as UEs that are far away from Node-B. Fast power control is used in WCDMA for link adaptation. On the contrary, HSDPA holds the transmission power constant over the TTI and uses adaptive modulation and coding (AMC) as an alternative link adaptation method to power control in order to improve the spectral efficiency which is defined as Kbits/s/MHz/cell in [15].

From the CQI reports as well as power measurement on the associated channels, the Node-B adjusts the data rate by modifying the modulation scheme, the effective code rate as well as the number of HS-PDSCH channelization codes. In a system with AMC, users close to the Node-B are typically assigned higher order modulation with higher code rates (e.g. 16 QAM with a 3/4 code rate), and the modulation-order and/or code rate generally decreases as the distance to the Node-B increases. Since 16-QAM is bandwidth efficient and requires greater received energy per bit, it is mainly suitable for low-dispersive channels close to Node-B. Consequently, rate adaptation mostly eliminates the need for power control. For services that tolerate short-term variations in the data rate, this method is more efficient than power control.

2.2.2 Hybrid-Automatic Repeat reQuest (H-ARQ)

To rapidly request the retransmission of erroneous transport blocks with substantial reduction in delay and increase in the efficiency of data retransmission, HSDPA adopts a H-ARQ mechanism which is based on stop-and-wait (SAW) protocol.

In SAW, the transmitting side persists on the transmission of the current block until the UE successfully receives it. In order to utilize the time when the Node-B awaits acknowledgements, N parallel SAW-ARQ processes may be set for the UE, so different processes transmit in separate TTIs. A practical value of N ranges between 4 and 6. The minimum delay between the original transmission and the first retransmission is 12 ms for HSDPA [14].

In HSDPA, the H-ARQ (Layer 1) is controlled from Node-B in contrast to from RNC in WCDMA. This eliminates the involvement of RNC for the storage of unacknowledged data packets and the following scheduling of retransmissions. Hence, the delay over the interface between the Node-B and RNC (i.e. the delay over Iub interface shown in Figure 1) is avoided and the resulting retransmission delay is significantly lower than the delay caused by conventional Radio Link Control (RLC) retransmissions. The retransmission might consist of the same set of coded bits as the initial transmission (Chase combining) or a different set of coded bits that represent the same information (incremental redundancy) [10].

The UE rapidly requests retransmission of data received in error. This substantially reduces delay and increases capacity compared to Release-99.

2.2.3 Packet Scheduling

The scheduler determines to which UE the shared channel transmission should be directed at any given moment. If the instantaneous channel condition to a UE is more favourable than others, data is transmitted to that UE.

For HSDPA, the medium access control sub-layer, MAC-hs (MAC for HSDPA), which also resides in the Node-B, executes the packet scheduling. This speeds up the packet scheduling decisions. Moreover, the shortened TTI length of 2 ms benefits the scheduling process.

A typically considered packet scheduling strategy is the Round-Robin in time scheduler where users are served in sequential order so that they all get the same average allocation time. However, the high scheduling rate combined with the large dynamic range of AMC available with the HSDPA concept also facilitates advanced scheduling methods where channel allocation is conducted according to the current radio conditions.

A popular advanced packet scheduling method is the proportional fair packet scheduler. With this type of scheduler, the serve order is determined by the highest relative instantaneous channel quality (RICQ – defined as the ratio between current and average E_s/N_0) and resources are allocated according to proportional fair algorithm. This method exploits short-term channel variations while maintaining long-term average user data rate [10], [14]. Ideally, users are scheduled only during constructive fades. It helps to achieve higher user data rate and increases overall cell throughput. Weighting the RICQ to buffer statistics can increase fairness of the algorithm [12] regardless of the qualities of the respective channels. In addition, traffic priorities can also be taken into account. As a result, scheduling based on both the channel quality and pre-assigned weights greatly increases system capacity and makes better use of resources over Round-Robin scheduling.

2.3 Spreading by OVSF Codes

Since WCDMA is designed to support a variety of data services from low to high bit rates, multiple rate transmission requires spreading codes of multiple spreading factors. In general, a code length of 2^{n-k} is needed for the bit rate of $2^k R_{min,}$ where n ranges from 2 to 9, k = 0, 1, …, n, and R_{min} corresponds to the bit rate associated with the lowest-bit-rate-service. Indeed, the supported data rate of each user varies inversely with the length

of the spreading code. In addition, orthogonal codes are used to improve the bandwidth efficiency (bits/Hz), with which more user bits can be transmitted. This enables high bit rate data transmission. Such codes are obtained by using modified Hadamard transformation and a tree structure as shown in Figure 5 and are called Orthogonal Variable Spreading Factor (OVSF) codes.

The characteristics of the OVSF codes are:

- OVSF codes preserve orthogonality between channels
- Each level in the code tree defines channelization codes of length SF
- All codes of the same level constitute a set: orthogonal to each other
- Any two codes of different levels are orthogonal if one code does not fall on the same lineage of the other. In essence, codes in the same lineage cannot be simultaneously used.

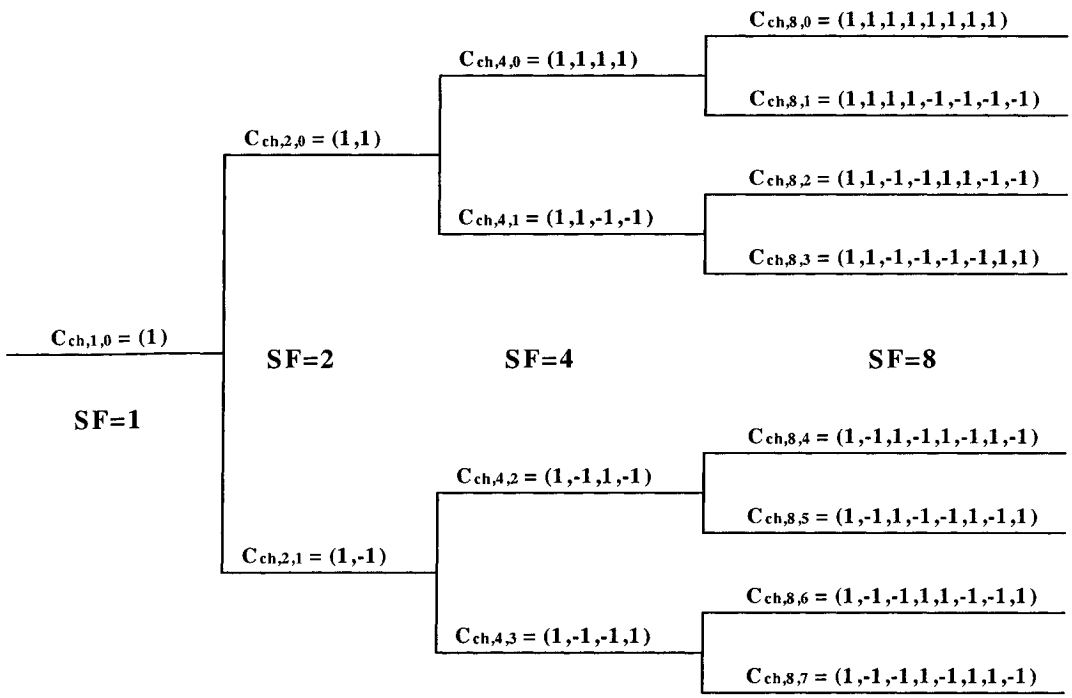

Figure 5: OVSF Codes Tree

The notation $C_{ch, SF, k}$ means the k_{th} code with the spreading factor SF. The leftmost value in each channelization codeword corresponds to the chip transmitted first in time.

OVSF codes of spreading factor 16 obtained using the generation method described above are tabulated in Table 2.

Table 2: OVSF Codes of SF=16

k	C_k(m), m=0. . SF-1															
1	1	1	1	1	1	1	1	1	1	1	1	1	1	1	1	1
2	1	1	1	1	1	1	1	1	-1	-1	-1	-1	-1	-1	-1	-1
3	1	1	1	1	-1	-1	-1	-1	1	1	1	1	-1	-1	-1	-1
4	1	1	1	1	-1	-1	-1	-1	-1	-1	-1	-1	1	1	1	1
5	1	1	-1	-1	1	1	-1	-1	1	1	-1	-1	1	1	-1	-1
6	1	1	-1	-1	1	1	-1	-1	-1	-1	1	1	-1	-1	1	1
7	1	1	-1	-1	-1	-1	1	1	1	1	-1	-1	-1	-1	1	1
8	1	1	-1	-1	-1	-1	1	1	-1	-1	1	1	1	1	-1	-1
9	1	-1	1	-1	1	-1	1	-1	1	-1	1	-1	1	-1	1	-1
10	1	-1	1	-1	1	-1	1	-1	-1	1	-1	1	-1	1	-1	1
11	1	-1	1	-1	-1	1	-1	1	1	-1	1	-1	-1	1	-1	1
12	1	-1	1	-1	-1	1	-1	1	-1	1	-1	1	1	-1	1	-1
13	1	-1	-1	1	1	-1	-1	1	1	-1	-1	1	1	-1	-1	1
14	1	-1	-1	1	1	-1	-1	1	-1	1	1	-1	-1	1	1	-1
15	1	-1	-1	1	-1	1	1	-1	1	-1	-1	1	-1	1	1	-1
16	1	-1	-1	1	-1	1	1	-1	-1	1	1	-1	1	-1	-1	1

The correlation properties of the OVSF codes determine the level of interference in WCDMA/HSDPA systems in general. The auto-correlation property affects the self-interference due to multipath propagation while the cross correlation affects the Multiple User Interference (MUI). OVSF codes are known to have poor correlation properties.

The auto-correlation of a code $x(t)$ of SF = N_c and chip duration T_c can be defined as

$$Rx(\tau) = \frac{1}{N_c T_c} \int_0^{NcTc} x(t)x(t-\tau)dt \qquad \textbf{Eq 2. 1}$$

In Figure 6, the auto-correlation of the 4th code from Table 2 is given. It is visible that the code does not have a single, narrow auto-correlation peak. Indeed, the non-peak auto-correlation is dependent on the actual codeword. Wider auto-correlation peak gives difficulty in synchronization.

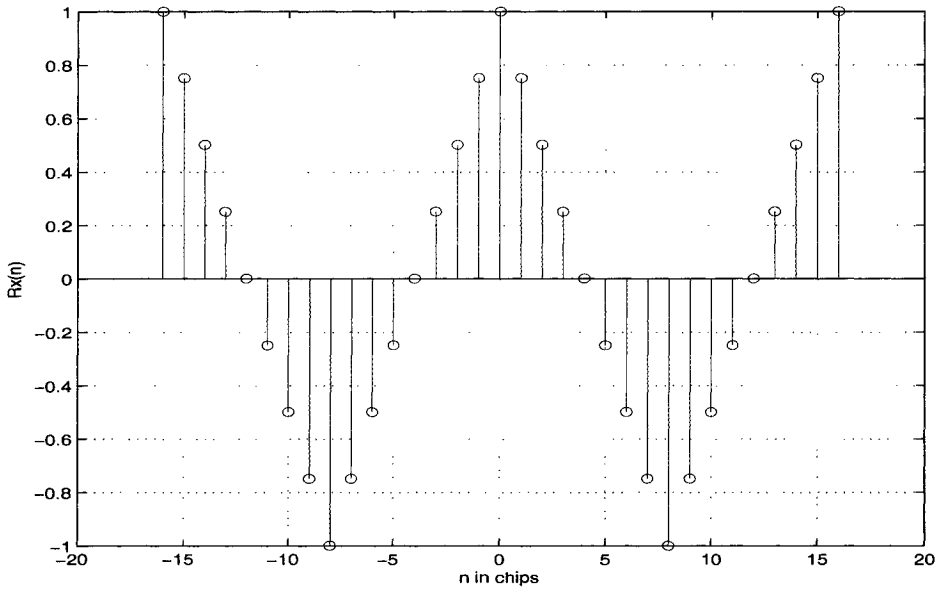

Figure 6: Auto-Correlation of 4th code in Table 2 (SF = 16)

Like wise, the cross-correlation of such sequences $x(t)$ and $y(t)$ can be defined as

$$Rxy(\tau) = \frac{1}{N_c T_c} \int_0^{NcTc} x(t)y(t-\tau)dt \qquad \textbf{Eq 2. 2}$$

The cross-correlation property of the OVSF codes is more important than the auto-correlation. There is zero cross correlation between the OVSF codes at zero lag; that is, perfect orthogonality is maintained only when codes are synchronous. However, OVSF codes have a significant cross correlation in case of non-alignment as the cross correlation between 4th and 6th codes from Table 2 shown in Figure 7. In fact, the cross-correlation is very much dependent on the particular pair of codes used; some have zero correlation while others have very high correlation.

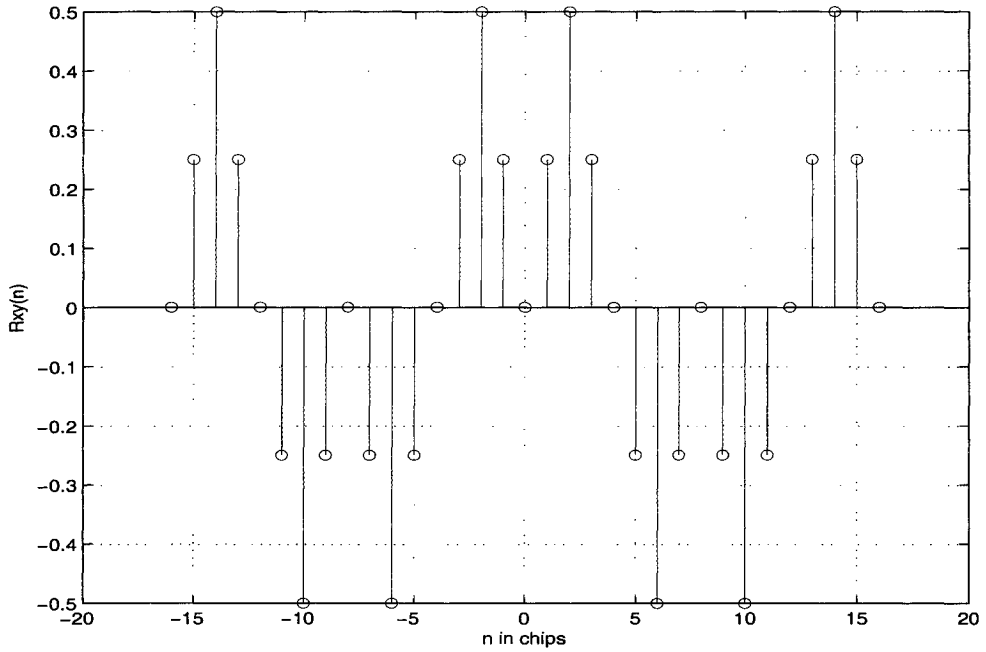

Figure 7: Cross-Correlation of 4th and 6th codes in Table 2 (SF = 16)

2.4 Generation of Scrambling Codes

Scrambling is an operation in which the spread chips are multiplied by a PN sequence called scrambling code. In the downlink of WCDMA (UTRA FDD), the scrambling codes are complex-valued Gold codes of length 2^{18}-1 truncated to form a cycle of a radio frame and are employed to uniquely distinguish cell sites. Moreover, these long codes serve the purpose of averaging the interference from other cells better.

In the case of HS-DSCH, the same scrambling code is applied to all HS-PDSCH channelization codes and HS-SCCH that a single UE may receive.

The scrambling code sequences are constructed by combining two real sequences into a complex sequence. Each of the two real sequences are constructed as the position wise modulo 2 sum of 38400 chip segments of two binary *m*-sequences generated using the primitive (over GF(2)) polynomials of degree 18. Suppose x and y are the two binary m-sequences. The x sequence is constructed using the primitive polynomial $1+X^7+X^{18}$. The

y sequence is constructed using the polynomial $1+X^5+X^7+X^{10}+X^{18}$. The resulting sequences thus constitute segments of a set of Gold sequences. The scrambling codes ($S_{dl,n}$) are repeated for every 10 ms radio frame.

The initial conditions for x and y are given by

$x(0) = 1, x(1) = x(2) = \ldots = x(16) = x(17) = 0$

$y(0) = y(1) = \ldots = y(16) = y(17) = 1.$

If $x(i)$ and $y(i)$ denote the ith symbol of the sequence x and y, respectively, then the subsequent symbols are generated recursively as follows:

$x(i+18) = x(i+7) \oplus x(i)$ $\quad i = 0,\ldots,2^{18}-20$

$y(i+18) = y(i+10) \oplus y(i+7) \oplus y(i+5) \oplus y(i)$ $\quad i = 0,\ldots, 2^{18}-20.$

The nth Gold code sequence z_n, $n = 0,1, 2, \ldots, 2^{18}-2$, is then defined as:

$z_n(i) = x((i+n) \text{ modulo } (2^{18} - 1)) + y(i) \text{ modulo } 2, i = 0,\ldots, 2^{18}-2.$

These binary sequences are converted to real valued sequences Z_n by the following transformation:

$$Z_n(i) = \begin{cases} +1 & \text{if } z_n(i) = 0 \\ -1 & \text{if } z_n(i) = 1 \end{cases} \quad \text{for} \quad i = 0,1,\ldots,2^{18} - 2.$$

Finally, the nth complex scrambling code sequence $S_{dl,n}$ is defined as:

$S_{dl,n}(i) = Z_n(i) + j\, Z_n((i+131072) \text{ modulo } (2^{18}-1)), i = 0,1,\ldots,38400$

2.5 Channel Coding (Error Control Coding)

Channel coding introduces redundancy in the transmitted data to protect them from errors. HS-DSCH channel coding uses the existing basic rate 1/3 Turbo code. Other code rates are generated from the basic rate 1/3 Turbo code by applying rate matching by means of puncturing or repetition.

2.6 Interleaving

When channel errors tend to occur in bursts, additional steps are required to maximize the performance of the coding process. One common technique is to scramble the channel bits prior to transmission by using an interleaver. Interleaving is a technique used to obtain time diversity without adding any overhead. Data interleaving alters a coded bit stream so as to minimize the effects of burst type channel degradations. By using this technique, adjacent bit errors caused by signal fades or bursts of interference are spread out in time across a longer interval, giving the decoder a greater probability of recovering the original data stream. There exist two popular forms of data interleaving: block interleaving and convolutional interleaving.

In WCDMA/HSDPA, interleaving is performed in two steps [16]:

1. The 1st interleaving is a block interleaver with inter-column permutations.
2. The 2nd interleaving is a block interleaver and consists of bits input to a matrix with padding, the inter-column permutation for the matrix, and bits output from the matrix with pruning.

2.7 Summary

The implementation of HSDPA is technically challenging because of its complexity and versatility. The complexity of HSDPA can be viewed from different angles: the complexity of the overall system and the computational complexity of a suitable receiver. HSDPA enabled UEs must be power-efficient and affordable, and deployment must not have a detrimental effect on already existing WCDMA performance. As mentioned in the beginning of the chapter, there are 12 UE categories that have been defined to support peak data rates ranging from 912 Kbit/s up to 14 Mbit/s in HSDPA. This implies different level of UE complexity.

The UE must be capable of

1. Processing for the hybrid-ARQ operation
2. Multi-code processing

3. HS-SCCH reception
4. HS-DPCCH signaling
5. Fast Turbo decoder processing

In highly dispersive radio channels, self-interference caused by multipath propagation limits the use of 16-QAM modulation as the required SNR is not obtainable. Although 16-QAM has limited robustness in WCDMA (i.e. CDMA) against interference, combining the link adaptation mechanism (scheduler prioritizes transmissions to UEs with favourable instantaneous channel conditions) mentioned above with it should yield higher carrier-to-interference ratio for the scheduled UE. In addition, the use of advanced receivers such as the G-RAKE receiver can suppress self-interference in order to compensate for performance losses.

CHAPTER 3

3. G-RAKE Receiver

3.1 Introduction

In a frequency-selective fading channel where the multipath delay spread is greater than the symbol period, the desired user's signal is not orthogonal to either its own delayed replica or the delayed replicas of other users' signals. Consequently, the overall interference (i.e. inter-cell and intra-cell interferences) becomes **coloured** (correlated).

In RAKE receiver, the interference due to cross-correlations with signals of different users is ignored or treated as white Gaussian noise. As a result, the system becomes interference-limited (the so-called *interference floor*). This limits the number of active users for particular BER and in turn the peak data rate in WCDMA/HSDPA. In order to compensate the performance degradation in such scenarios, G-RAKE combines the intra-cell and inter-cell interferences as coloured Gaussian noise at the fingers' output.

The structure of a G-RAKE receiver is depicted in Figure 8 and is very similar to the conventional RAKE receiver as the one shown in Figure 39 in the Appendix A.6.

The Maximum Ratio Combining (MRC) in RAKE is optimum only if the aggregate noise plus interference in each finger output has equal power and appear uncorrelated. However, the use of OVSF codes in WCDMA makes it difficult to meet those conditions as for reasons mentioned in section 2.3 of the previous chapter. As such, the G-RAKE determines the aggregate noise plus interference powers on different fingers and correlation among them by averaging over the aperiodic cross-correlation function of the spreading sequence (i.e. the OVSF codes combined with scrambling code). From these noise properties (i.e. covariance matrix), the combining weights w_j are calculated by Maximum Likelihood (ML) formulation, where $j = 0, 1, \ldots, J$ and J being the total number of G-RAKE fingers.

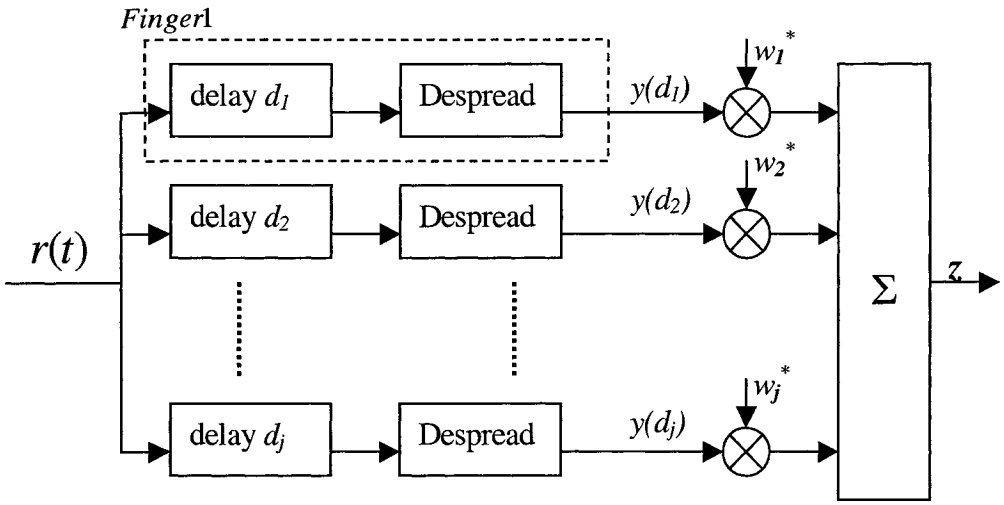

Figure 8: G-RAKE Receiver Architecture

The number of fingers in a RAKE is the same as the number of multipath components, which is typically determined by searching through different paths (from the power delay profile of the received signal). The G-RAKE, however, uses more fingers than the number of multipath components. It is stated that a suitable choice for J to achieve most of the performance gain is less than or equal to $2L$, where L is the number of multipaths [4]. The role of these extra fingers can be viewed as producing inverse channel filtering effect as briefed in [4]. Consequently, these fingers play the role of canceling the overall interference. Moreover, the finger delays d_j are chosen to maximize the SINR of the decision statistics z at the output of the receiver.

To better explain the details of the G-RAKE receiver, a practical HSDPA transmission scheme is developed in section 3.2. The corresponding received signal for the transmitted signal that travels through a multipath channel is derived in section 3.3. A detail mathematical analysis of the ML approach to calculate the combining weights for the received signal is presented in section 3.4. The G-RAKE receiver's finger placement methods found in the literature are described in section 3.5. Finally, a summary of how

finger delays and weighting coefficients are determined in the simulation of this thesis is given in section 3.6.

3.2 HSDPA Transmit Structure

Typically, the transmitter for the HSDPA combines different downlink physical channels (i.e. SCH, HS-SCCH, DPCH, HS-PDSCH) by complex addition before being pulse-shaped and sent over a single carrier [17].

In what follows, only HS-PDSCH channels are considered. The shared OVSF codes with SF = 16 are mapped onto these physical channels and 16-QAM modulation scheme is employed. In order to simplify the HSDPA system, the following are assumed in the processing of Transport Blocks (TB) of data bits.

- Typically, the number of active users supported by a WCDMA multi-code system is small as it is meant for high-speed data transmissions with high transmit power. To simplify the analysis, it is assumed that all or a subset of the available 15 codes may either be assigned to a single user or be allocated to multiple users. When a single user is assigned all or a subset of codes, the interference will be referred to as Multi-Code Interference (MCI). If all or subsets of codes are shared among multiple users, the interference will be referred to as Multiple User Interference (MUI).
- Single cell is considered.
- Single Node-B is considered.
- CRC attachment, channel coding, interleaving and rate matching are not performed; that is, raw source bits are injected into the transmitter.
- Modulating chip rate is 3.84 Mchips/s as stated in [13].
- The carrier frequency of 2 GHz is assumed throughout this study as specified in [15] for UMTS band applications.

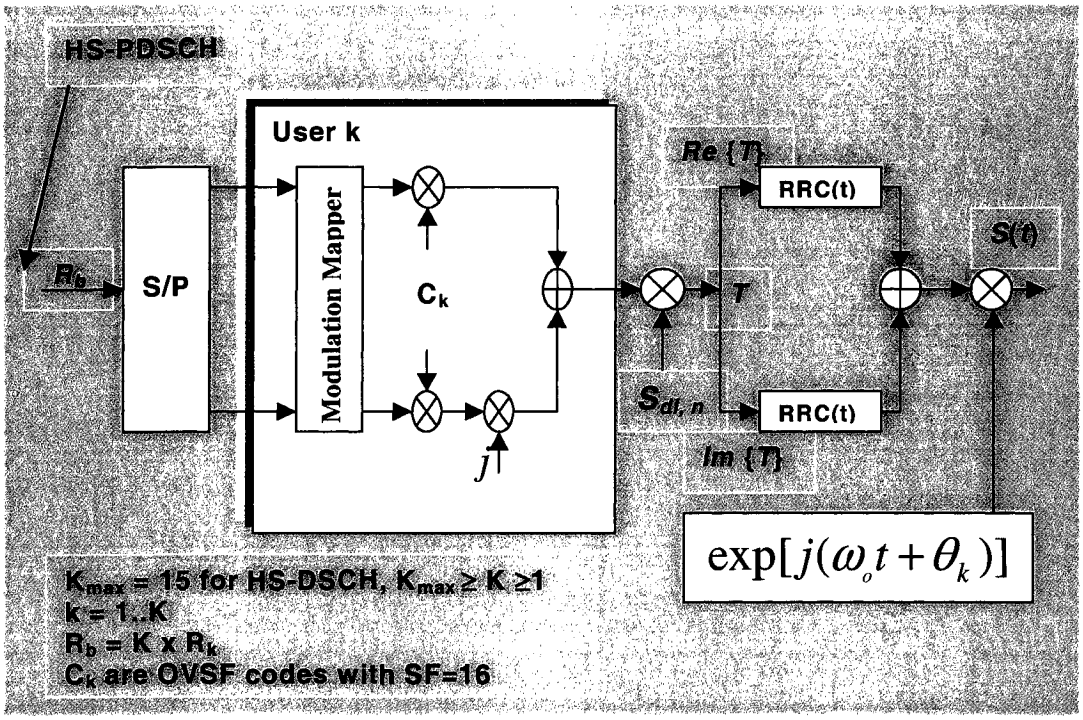

Figure 9: Simplified HSDPA Tx Structure

As depicted in Figure 9, a set of consecutive binary symbols are split into *K* parallel streams (i.e. serial-to-parallel conversion) and mapped to an I and Q branch to have the signal constellation as shown in Figure 10 before being spread by parallel orthogonal channelization codes.

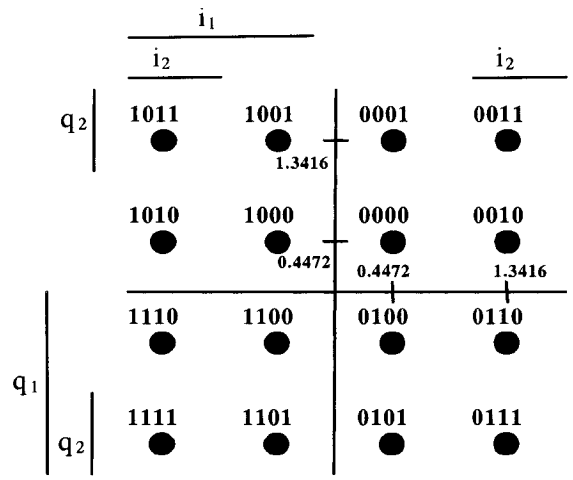

Figure 10: 16-QAM Constellation

It is noticeable that each adjacent symbol differs by only one bit; that is, gray-coding is used to map data to constellation points as depicted in Figure 10. The resulting modulation mapper is defined in Table 3.

Table 3: 16-QAM Modulation Mapping

$i_1q_1i_2q_2$	I branch	Q branch
0000	0. 4472	0. 4472
0001	0. 4472	1. 3416
0010	1. 3416	0. 4472
0011	1. 3416	1. 3416
0100	0. 4472	-0. 4472
0101	0. 4472	-1. 3416
0110	1. 3416	-0. 4472
0111	1. 3416	-1. 3416
1000	-0. 4472	0. 4472
1001	-0. 4472	1. 3416
1010	-1. 3416	0. 4472
1011	-1. 3416	1. 3416
1100	-0. 4472	-0. 4472
1101	-0. 4472	-1. 3416
1110	-1. 3416	-0. 4472
1111	-1. 3416	-1. 3416

In reality, each symbol is spread to the chip rate by the corresponding real-valued channelization code C_k. The channelization codes assigned in each stream are essentially OVSF codes that preserve the orthogonality between a user's different physical channels as described in section 2.3. In this study, the user-specific OVSF codes (i.e. Walsh-Hadamard sequences) of spreading factor 16, the process of which construction is already shown in section 2.3, are used.

The output of this channelization process in each HS-PDSCH is a single complex-valued sequence of chips. This sequence of chips from all multi-codes is linearly summed to produce a single composite complex-valued sequence of chips. The composite chips sequence then undergoes scrambling by means of Node-B specific scrambling code, $S_{dl,n}$, generated as outlined in section 2.4.

The scrambled chip sequence, corresponding to point T in Figure 9 above, is passed through a RRC pulse-shaping filter of roll-off factor 0.22 with impulse response $p(t)$, which is shown in Figure 11.

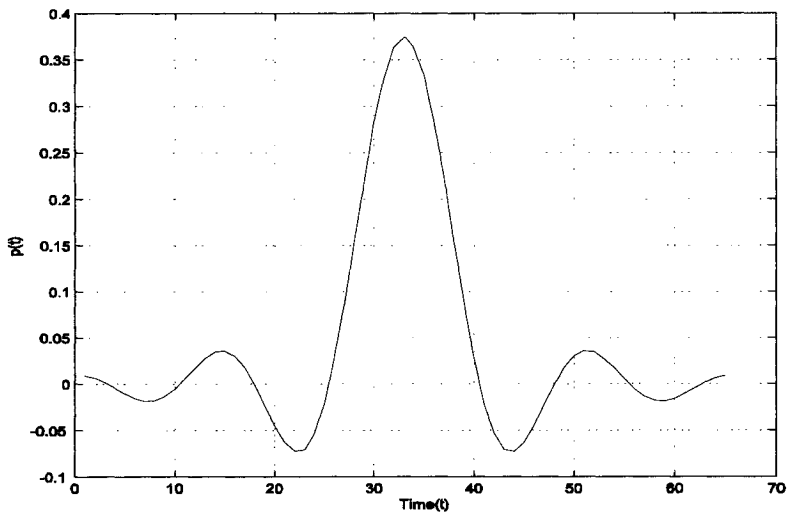

Figure 11: RRC Pulse (FIR Filter) with $\alpha = 0.22$

The auto-correlation of the RRC pulse $p(t)$ is shown in Figure 12. It is indeed a raised-cosine response.

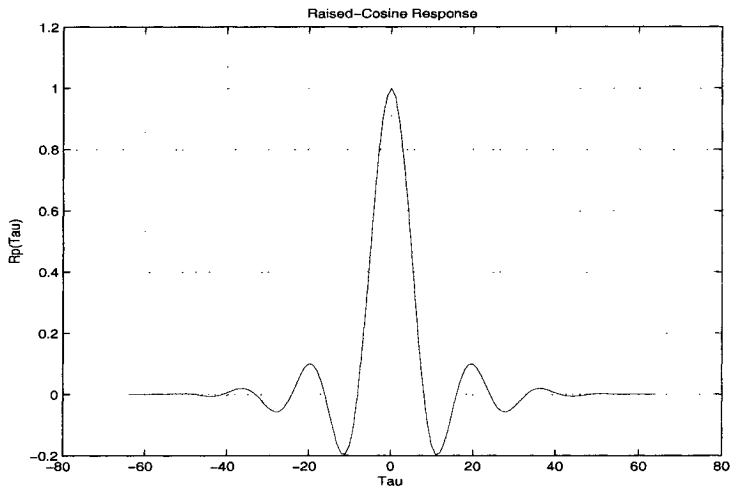

Figure 12: Auto-Correlation of RRC Pulse $p(t)$

Typically, the RRC filter must operate at a sample rate of no less than twice the data rate to span the frequency response characteristic of the raised cosine pulse. However, to provide a more accurate spectral shape, it is desirable to oversample the input data

sequence by a factor of eight. As such, the RRC filter in Figure 11 is designed to span 8 chips (8 samples/chip x 8 chips = 64 samples); that is, if F_s is the sampling frequency for the filter and F_d is the sampling frequency of the input chip sequence, F_s/F_d is chosen to be 8. As can be seen from the above figures, the order (i.e. pulse length) of the RRC filter is chosen to be 65 to avoid half-chip delay associated with an even number of taps.

The baseband equivalent of the transmitted signal resulting from above operations can be mathematically expressed by the following equation for K synchronous multi-code WCDMA system.

$$s(t) = \sum_{i=-\infty}^{\infty} \sum_{k=1}^{K} \sqrt{E_k} d_k(i) \sum_{m=0}^{N-1} C_{k,i}(m) p(t - iT - mT_c) \qquad \textbf{Eq 3. 1}$$

Here, T_c is the chip duration, $T = N T_c$ is the symbol duration, E_k is the energy per symbol of kth stream, and $d_k(i)$ is the ith source symbol in kth stream and maps to one of the 16 constellations in Table 3. The scaling factor used to normalize the average energy is $\sqrt{\frac{(M-1)}{3}}$, where M = 16 for 16-QAM.

In effect, each symbol $d_k(i)$ is spread by user-specific and symbol period dependent complex spreading sequence $C_{k,i}(m) \in \left\{ \pm \frac{1}{\sqrt{2N}} \pm \frac{1}{\sqrt{2N}} \right\}$, m = 0, . . . , ($N$-1), where N denotes the spreading factor. Note that the complex spreading sequence combines the product of the user-specific OVSF code and the Node-B-specific long scrambling code. The factor $\frac{1}{\sqrt{N}}$ comes from normalization of each OVSF code so that the bit energy is preserved before and after the spreading. Hence, the energy is normalized for one symbol.

3.3 Received Signal

At the mobile front end, the received signal that has propagated through the multipath channel is

$$r_F(t) = \sum_{l=0}^{L} h(l)s(t-\tau_l) + n(t) \qquad \textbf{Eq 3. 2}$$

where L is the number of multipaths, τ_l is the delay for the lth path, $h(l)$ is the complex-valued channel coefficient for the lth path, and $n(t)$ is AWGN with single-sided power spectral density N_o. Here, $n(t)$ models the inter-cell interference and the thermal noise.

This received signal is first passed through a chip-matching filter that matches the transmitter filter. In this analysis, the same RRC pulse shown in Figure 11 is used as the chip-matching filter to realize overall raised-cosine pulse shape. By doing so the SNR at the receiver is maximized. The output of the receiving filter (chip-matching filter) is expressed as

$$r(t) = \int p^*(\lambda - t) r_F(\lambda) d\lambda \qquad \textbf{Eq 3. 3}$$

where the integral represents the convolution of $p^*(t)$ with $r_F(t)$ and * denotes the complex-conjugate.

The output is downsampled by a factor of 8 to match the chip rate. For the transmitted signal $s(t)$, given in Eq 3.1, the expression in Eq 3.3 can be shown as

$$r(t) = \sum_{k=0}^{K-1} \sum_{l=0}^{L-1} \sum_{i=-\infty}^{\infty} \sqrt{E_k} h(l) d_k(i) R_{k,i}(t - iT - \tau_l) + z(t) \qquad \textbf{Eq 3. 4}$$

where $z(t)$ is the filtered noise and $r(t)$ is the baseband signal to be despread by the G-RAKE receiver, integrated and dumped, and combined to produce decision statistics.

The triple summation in $r(t)$ consists of both the desired signal and interference (MUI + ISI).

In the following, steps involved in processing the received signal by the G-RAKE receiver in order to decode the transmitted information are explained.

3.4 Combining Weights

The despreading operation is such that the received chip sequence in each finger is multiplied by the set of known OVSF codes, and the result is integrated over one symbol period to produce signal constellations. The finger outputs of the despreading operation of the received signal given in Eq 3.4 can be expressed in vector notations as

$$\mathbf{y} = \mathbf{h}s_0(0) + \mathbf{u} \qquad \textbf{Eq 3. 5}$$

where $\mathbf{y} = [y(d_1), y(d_2), ..., y(d_J)]^T$ is a vector containing the signal after despreading, $s_0(0)$ is the symbol of interest (the symbol 0 of user #0), and $\mathbf{h}$ is a vector of complex values formed by channel responses and pulse shaping function. The vector $\mathbf{u}$ models the overall noise consisting of AWGN noise and interference from both intra-cell and inter-cell. Thus,

$$\mathbf{u} = \mathbf{y} - \mathbf{h}s_0(0) = \mathbf{n}_{MAI} + \mathbf{n}_{TH} \qquad \textbf{Eq 3. 6}$$

where $\mathbf{n}_{MAI}$ and $\mathbf{n}_{TH}$ represent the overall interference (from intra-cell and other cells) and thermal noise, respectively.

As a whole, $\mathbf{u}$ is a vector containing complex-valued Gaussian random variables that are correlated (coloured) and has a PDF of the form given in Eq A.3 in the Appendix. Hence, the PDF of $\mathbf{u}$ can be written as

$$p_u(\mathbf{u}) = \frac{1}{\pi^J |\mathbf{R_u}|} e^{\left[-\mathbf{u}^H \mathbf{R_u}^{-1} \mathbf{u}\right]} \quad \text{Eq 3. 7}$$

In the above equation, a J dimensional Gaussian PDF with zero mean and covariance $\mathbf{R_u}$ describes the coloured-noise. Here, H denotes the transpose and conjugate operation, J is the number of fingers, and $\mathbf{R_u}$ is the covariance matrix of $\mathbf{u}$ defined as

$$\mathbf{R}_u = E[\mathbf{u}\mathbf{u}^H] = E[(\mathbf{y} - \mathbf{h}s_0(0))(\mathbf{y} - \mathbf{h}s_0(0))^H] \quad \text{Eq 3. 8}$$

where $E[.]$ denotes the expected value.

Replacing $\mathbf{u}$ in Eq 3.7 with the expression given in Eq 3.6, the G-RAKE finger output vector $\mathbf{y}$ is described by a J dimensional Gaussian PDF with mean $\mathbf{h}s_0(0)$ and covariance $\mathbf{R_u}$ as follows:

$$p(\mathbf{u} = \mathbf{y} - \mathbf{h}s_0(0)) = \frac{1}{\pi^J |\mathbf{R_u}|} e^{\left[-(\mathbf{y} - \mathbf{h}s_0(0))^H \mathbf{R_u}^{-1} (\mathbf{y} - \mathbf{h}s_0(0))\right]} \quad \text{Eq 3. 9}$$

Assuming the knowledge of $\mathbf{h}$, the above equation can be restated as

$$p(\mathbf{y} \mid s_0(0)) = \frac{1}{\pi^J |\mathbf{R_u}|} e^{\left[-(\mathbf{y} - \mathbf{h}s_0(0))^H \mathbf{R_u}^{-1} (\mathbf{y} - \mathbf{h}s_0(0))\right]} \quad \text{Eq 3. 10}$$

The conditional PDF $p(\mathbf{y}|s_0(0))$ is the likelihood function. If it is assumed that the symbol $s_0(0)$ is equally probable a priori (i.e. $P(s_m(0)) = 1/M$, m=1, 2,..., M), the decision rule is based on finding the symbol $s_0(0)$ that maximizes $p(\mathbf{y}|s_0(0))$. This decision criterion based on the maximum of $p(\mathbf{y}|s_0(0))$ over the M signals is called the maximum-likelihood (ML) criterion. Furthermore, the above equation can conveniently be expressed in natural logarithm as

$$\ln[p(\mathbf{y} \mid s_0(0))] = \ln[\pi^{-J} |\mathbf{R_u}|^{-1}] - [(\mathbf{y} - \mathbf{h}s_0(0))^H \mathbf{R_u}^{-1} (\mathbf{y} - \mathbf{h}s_0(0))] \quad \textbf{Eq 3. 11}$$

The maximum of $\ln[p(\mathbf{y}|s_0(0))]$ is equivalent to finding the minimum of the log-likelihood function

$$\Lambda(s_0(0)) = (\mathbf{y} - \mathbf{h}s_0(0))^H \mathbf{R_u}^{-1} (\mathbf{y} - \mathbf{h}s_0(0)) = \mathbf{u}^H \mathbf{R_u}^{-1} \mathbf{u} \quad \textbf{Eq 3. 12}$$

Essentially, the result of the minimization of Eq 3.12 yields in the estimation of $s_0(0)$ from the decision statistic as

$$\hat{s}_0(0) = \mathbf{w}^H \mathbf{y} \quad \textbf{Eq 3. 13}$$

where $\mathbf{w} = [w_1, w_2, ..., w_J]^T$ is the vector containing the optimal combining weights for the G-RAKE receiver.

Further expansion of Eq 3.12 gives

$$\Lambda(s_0(0)) = (\mathbf{y}^H \mathbf{R_u}^{-1} \mathbf{y} - 2\mathrm{Re}(s_0(0)^* \mathbf{h}^H \mathbf{R_u}^{-1} \mathbf{y}) + |s_0(0)|^2 \mathbf{h}^H \mathbf{R_u}^{-1} \mathbf{h} \quad \textbf{Eq 3. 14}$$

where Re(.) denotes the real part .

Substitution of Eq 3.14 into Eq 3.9 results in

$$p(\mathbf{u} = \mathbf{y} - \mathbf{h}s_0(0)) = Ce^{\left[2\mathrm{Re}(s_0(0)^* \mathbf{h}^H \mathbf{R_u}^{-1} \mathbf{y}) - |s_0(0)|^2 \mathbf{h}^H \mathbf{R_u}^{-1} \mathbf{h}\right]}$$

$$p(\mathbf{u} = \mathbf{y} - \mathbf{h}s_0(0)) = Ce^{\left[2\mathrm{Re}(s_0(0)^* \mathbf{w}^H \mathbf{y}) - |s_0(0)|^2 \mathbf{w}^H \mathbf{h}\right]} \quad \textbf{Eq 3. 15}$$

where C is a constant independent of the symbol of interest.

The combining weights, $\mathbf{w}$, in Eq 3.15 are determined as

$$\mathbf{w} = \mathbf{R}_u^{-1}\mathbf{h} \qquad \textbf{Eq 3. 16}$$

This shows that the optimal combining weights for the G-RAKE depend on both the covariance matrix and the channel response.

Effectively, the estimation of the symbol of interest, $s_0(0)$, is achieved by maximizing the log-likelihood function, $\ln[p(\mathbf{y}|s_0(0))]$, of the G-RAKE fingers' outputs (i.e. despread signal) $\mathbf{y}$.

As mentioned above, the covariance matrix $\mathbf{R}_u$ characterizes how the interference is correlated from channel to channel. It can be constructed from covariance matrices of MUI and ISI caused by users from within the cell as expressed in [4]. Thus,

$$\mathbf{R}_u = E_0\mathbf{R}_{ISI} + E_I\mathbf{R}_{MUI} + N_0\mathbf{R}_n \qquad \textbf{Eq 3. 17}$$

where $\mathbf{R}_{ISI}$ is a covariance matrix due to the ISI, $\mathbf{R}_{MUI}$ is a covariance matrix due to the MUI, $\mathbf{R}_n$ is the covariance matrix of additive noise, E_0 is the average energy of the symbol of interest, and E_I is the total energy of the interference symbols . Furthermore, the elements of $\mathbf{R}_{ISI}$, $\mathbf{R}_{MUI}$, and $\mathbf{R}_n$ can be computed using the series solution presented in [4].

3.5 Placement of G-RAKE Fingers

One of the characteristics of the G-RAKE receiver is that it utilizes more fingers than the number of multipaths to suppress interference. However, inclusion of additional fingers increases the complexity of extra correlator despreading and in turn the calculation of the combining weights (i.e. larger size of the covariance matrix). It is proven in the literature that better performance is achieved as the number of fingers approaches twice the number of resolvable multipaths [4]-[7].

G-RAKE benefits from fingers not corresponding to channel rays. Finger placement in G-RAKE is a trade-off between matching to the channel and whitening the coloured noise. When the first L fingers are placed on the multipath components through conventional finger search, the channel is matched. Placement of additional fingers can be characterized as having a physical interpretation of a whitening matched filter (WMF). This can be viewed through the **Cholesky factorization** of the covariance matrix $\mathbf{R_u}$ or its inverse $\mathbf{R_u}^{-1}$ (for symmetric positive-definite matrix). With the factorization $\mathbf{R_u} = \mathbf{L}\mathbf{L}^H$ ($\mathbf{L}$ is the lower triangular part of $\mathbf{R_u}$), the expression for the combining weights $\mathbf{w}$ can be written as

$$\mathbf{w} = \mathbf{R}_u^{-1}\mathbf{h} = (\mathbf{L}^{-1})^H (\mathbf{L}^{-1}\mathbf{h}) \qquad \textbf{Eq 3. 18}$$

The first term $(\mathbf{L}^{-1})^{-H}$ acts like a (possibly time-varying) **whitening filter (inverse channel filter)** of the overall interference $\mathbf{u}$ since $E[(\mathbf{L}^{-1}\mathbf{u})(\mathbf{L}^{-1}\mathbf{u})] = \mathbf{I}$ (identity matrix) [5]. The second term is the **matched filter** (MF). In effect, the G-RAKE can be viewed as a combination of a pre-whitening filter followed by a matched filter. When the additional fingers are placed on the strongest taps of the inverse channel filter, the coloured noise is whitened and thus suppresses interference effectively.

Now, the challenging task is to locate these additional finger positions. There is a method outlined in [4] that searches in a window of potential delays for the finger positions that yield maximum output SNR of the G-RAKE, where SNR is defined as

$$SNR = \frac{\mathbf{w}^H \mathbf{h}\mathbf{h}^H \mathbf{w}}{\mathbf{w}^H \mathbf{R}_u \mathbf{w}} \qquad \text{Eq 3. 19}$$

This optimal finger placement is not straightforward and practically complex. This leaves us with no closed-form expression for finding the finger delays.

However, a simpler and more practical strategy resulting in low complexity and good performance is proposed to allocate the extra G-RAKE fingers [5]. The idea behind this strategy is to cancel the interference induced on each multipath by placing extra fingers in symmetrical places around that path.

According to this scheme, the first *L* fingers are positioned on the actual *L* dominant multipath components. Then, those L fingers are sorted according to their energy and corresponding timings are stored in an array. Additional *J-L* fingers are placed around each dominant multipath, starting from the strongest to the weakest. In doing so, it is ensured that the position of the new finger is not too close to another already existing finger in order to achieve maximum diversity.

For example, Figure 13 shows one possible finger placement for a 4-ray multipath channel. In case the first multipath is not the strongest, the remaining *J-L* fingers probably may end up in different set of positions.

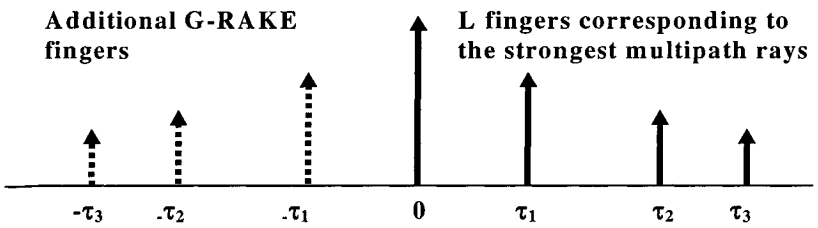

Figure 13: Less Complex G-RAKE Finger Placement Scheme

3.6 Summary

As explained before, no close form solution is available for determining the optimal finger delays for the G-RAKE receiver. It is a trade-off between matching to the channel and canceling the interference caused by the multipath channel. This work primarily depends on the finger placement scheme suggested in [4]; that is, different combinations of finger positions that yield relatively higher SNR (at the receiver output) are chosen for our analysis when the channel is time-invariant. From this, the finger combination that gives the maximum SNR can be isolated and can be used to find the corresponding BER performance of the G-RAKE receiver. For time-variant channels, either the maximum instantaneous SNR or the minimum BER averaged over the fading channel coefficients is used to decide the finger locations.

For each finger combination, the channel impairment matrix (covariance matrix) is calculated according to the formula given in Eq 3.17. Then, using Eq 3.16, the G-RAKE weighting coefficients are estimated assuming perfect knowledge of the channel.

CHAPTER 4

4. Complexity Issues

4.1 Introduction

To calculate the combining weights **w** in Eq 3.16, the following linear system of J equations in J unknowns has to be solved.

$$\mathbf{R}_u\mathbf{w} = \mathbf{h} \qquad \text{Eq 4. 1}$$

Traditionally, this is achieved by matrix inversion techniques such as Gauss-Jordan Elimination (GJE) (or Gaussian Elimination) and LU Decomposition (LUD). Matrix inversion is one of the most computationally intensive tasks. The two main innermost loops of the GJE algorithm, each containing one subtraction and one multiplication, are each executed J^3 times (J is the number of fingers). This configuration yields floating-point operations count of $2J^3$ and a computational complexity of $O(J^3)$. Matlab's matrix inversion method performs LUD and column-by-column forward and backward substitution. LU decomposition of the matrix into its triangular factors requires $2J^3/3$ operations. And, the *forward substitution* and *backward substitution* require $J^3/3$ and J^3 operations, respectively. Hence, the total operations count is $2J^3$, just as in the case of GJE. The overall computational complexity is, therefore, $O(J^3)$ [18]. And, the memory requirement is $O(J^2)$. Because these methods theoretically produce the exact solution, they are commonly referred to as Direct Methods.

An alternative to the above is the so-called iterative methods (or indirect methods) that are economical in terms of execution time and memory utilization. Noticeably, $\mathbf{R}_u$ is most of the time a sparse matrix (~1/3 of zeros in the matrix), which further helps reducing the amount of calculation in iterative methods whereas the Direct Methods cannot exploit this structure.

In section 4.2, an indirect method called the Gauss-Seidel iterative technique to solve for the G-RAKE combining weights is described, which includes a brief analysis of its computational complexity. Likewise, the Conjugate Gradient algorithm to iteratively solve for the G-RAKE combining weights is explained in section 4.3. Finally, a comparison of both these methods in terms of their computational aspects is made in section 4.4.

4.2 Gauss-Seidel Iterative Method

The Gauss-Seidel (GS) iterative method is one of the widely used techniques to solve Eq 4.1 shown above [18]. This method is applicable to

(a) strictly diagonally dominant

$$|\mathbf{R}_u(i,i)| > \sum_{j=1}^{i-1} |\mathbf{R}_u(i,j)| + \sum_{j=i+1}^{J} |\mathbf{R}_u(i,j)| \qquad \textbf{Eq 4. 2}$$

where i = 1, 2, 3, ..., J and $|\,.\,|$ denotes the absolute value.

(b) symmetric positive definite (Hermitian Symmetric Positive Definite)

matrices. The GS method always converges if either (a) or (b) is true.

In terms of matrices, the definition of the Gauss-Seidel method for $\mathbf{R}_u$ can be expressed as

$$(\mathbf{D}+\mathbf{L})\mathbf{w}_{n+1} = \mathbf{h} - \mathbf{L}^H\mathbf{w}_n \qquad \textbf{Eq 4. 3}$$

where $\mathbf{R}_u = \mathbf{L}+\mathbf{D}+\mathbf{L}^H$, and $\mathbf{D}$ and $\mathbf{L}$ are the main diagonal and strictly lower triangular parts of $\mathbf{R}_u$.

The computational costs per iteration step amount to roughly $2J^2$ operations (additions, subtractions, multiplications), plus J^2 operations for the solution of the lower triangular system $\mathbf{L}$: in total $3J^2$ operations per iteration step. The overall computational complexity is in the order of $O(J^2)$. The storage space required is roughly $(J + m)$ where m is the non-zero elements in $\mathbf{R}_u$.

In general, the convergence of this iterative method can be accelerated by using Successive Over-Relaxation (SOR). It is a technique used to accelerate any iterative procedure by arbitrarily correcting the intermediate values of the unknowns in the anticipated direction before the next iteration, and this is done according to the form

$$(\mathbf{D} + \omega\mathbf{L})\mathbf{w}_{n+1} = \omega\mathbf{h} - (\mathbf{L}^H + (1 - \omega)\mathbf{D})\mathbf{w}_n \qquad \textbf{Eq 4. 4}$$

where ω is the relaxation parameter, the range of which is restricted to $0 < \omega < 2$ [19]. For faster convergence, ω should be chosen between 1 and 2. If $\omega = 1$, the SOR method simplifies to the Gauss-Seidel method. An optimum value for over relaxation parameter can be found by trial-and-error.

4.3 Conjugate Gradient Iterative Method

Another popular iterative technique for solving symmetric positive definite matrices is the Conjugate Gradient (CG) method of Hestenes and Stiefel [20]. The CG method derives its name from the fact that it generates a sequence of conjugate (or orthogonal) vectors. These vectors are the residuals of the iterates. They are also the gradients of a quadratic function, the minimization of which is equivalent to solving the linear system. The method proceeds by generating vector sequences of iterates (i.e. successive approximations to the solution), residuals corresponding to the iterations, and search directions used in updating the iterates and residuals.

The convergence rate of the CG method is determined by the condition number of $\mathbf{R}_u$, $K(\mathbf{R}_u) = \det(\mathbf{R}_u)\det(\mathbf{R}_u^{-1})$, which is closely related to the distribution of eigenvalues of $\mathbf{R}_u$. In exact arithmetic, the algorithm is as follows:

Input: $\mathbf{w}_0 = \mathbf{0}$, $\mathbf{r}_0 = \mathbf{h}$, $\mathbf{d}_0 = \mathbf{r}_0$
Output: exact solution $\mathbf{w}$

for k = 1, 2,..., J

$$\begin{cases} \alpha_k = \dfrac{\mathbf{r}_k^T \mathbf{r}_{k-1}}{\mathbf{d}_{k-1}^T \mathbf{R}_u \mathbf{d}_{k-1}} & \text{step length} \\ \mathbf{w}_k = \mathbf{w}_{k-1} + \alpha_k \mathbf{d}_{k-1} & \text{approximate solution} \\ \mathbf{r}_k = \mathbf{r}_{k-1} - \alpha_k \mathbf{R}_u \mathbf{d}_{k-1} & \text{residual} \\ \beta_k = \dfrac{\mathbf{r}_k^T \mathbf{r}_k}{\mathbf{r}_{k-1}^T \mathbf{r}_{k-1}} & \text{improvement} \\ \mathbf{d}_k = \mathbf{r}_k + \beta_k \mathbf{d}_{k-1} & \text{search direction} \end{cases}$$

The CG method involves one matrix-vector product, three vector updates, and two inner products per iteration. Therefore, the work per iteration is $5J$ multiplications plus one matrix-vector product. Like most iterative methods, CG has modest storage requirements; storage is required for four vectors of length J in addition to the static storage required for $\mathbf{R}_u$. CG computes the solution in a maximum of J steps in exact arithmetic.

The Preconditioned Conjugate Gradient (PCG) method [20]-[22] is a generalization of the classic CG method. In effect, it increases the rate of convergence of the basic CG method. The goal of preconditioning is to convert the original system into an equivalent one that has a (much) lower condition number. For preconditioning to be effective, the faster convergence must overcome the added costs of applying the preconditioning, so that the total cost of solving the linear system is lower.

One widely used class of preconditioning is the incomplete $\mathbf{LDL}^H$ factorizations. The Symmetric Successive Over-Relaxation (SSOR) preconditioning scheme belongs to this class. No additional computing time is required for constructing the SSOR preconditioning matrix, and it contains more global information of the $\mathbf{R}_u$ matrix [22]-[23]. In the SSOR preconditioning scheme, the preconditioner $\mathbf{C}$ is chosen as follows:

$$\mathbf{C} = (\mathbf{D} + \mathbf{L})\mathbf{D}^{-1}(\mathbf{D} + \mathbf{L}^H) \qquad \text{Eq 4. 5}$$

The efficient implementation of SSOR in the CG algorithm can speed up the convergence roughly five times faster. Moreover, splitting $\mathbf{C}$ into $\mathbf{C1} = \mathbf{D}+\mathbf{L}$ and $\mathbf{C2} = \mathbf{D}^{-1}*(\mathbf{D}+\mathbf{L}^H)$ buys computational advantage. The total cost of the SSOR PCG iteration is $(8J + m)$ per iteration [22]. An additional J words of storage is required over classic CG method. Overall, the complexity is almost the same as the classic CG method without preconditioning.

4.4 Computational Aspects and Summary

In this section, the order of execution and storage requirement per iteration for each of the iterative methods described above are summarized.

Table 4: Computational Complexity of Iterative Methods

Iterative Method	Order of execution	Storage
GS	$O(J^2)$	Covariance Matrix + J
SOR	$O(J^2)$ or less	Covariance Matrix + $2J$
CG	$O(J^2)$ or less Depends on the number of distinct eigen values and condition number of $\mathbf{R}_u$	Covariance Matrix + $4J$
SSOR-PCG	$O(J^2)$ or less	Covariance Matrix + $5J$

The computational complexity of all the methods listed in Table 4 is roughly about the same with modest memory storage as the size of the covariance matrix is small. Difference in computational complexity will become noticeable when the covariance matrix is bigger. However, CG/PCG methods are preferred over GS/SOR methods because of their robust convergence behaviour.

CHAPTER 5

5. G-RAKE Performance Analysis

5.1 Introduction

In this chapter, the performance of the G-RAKE receiver in terms of BER is investigated through simulation. It also includes simulation experiments for the complexity reduction techniques discussed in the previous chapter.

Various multipath fading channel responses that are used in the simulation are presented in section 5.2. Simulation results in each of these fading environments are presented and discussed in section 5.3.

5.2 Channel Types

Two types of multipath channels are used in the link level performance analysis: time-invariant channel and time-variant channel.

5.2.1 Time-Invariant Channel

The following fixed coefficient channel is used in the literature [4] for the G-RAKE receiver performance analysis using QPSK modulation and spreading factor of 128.

Table 5: Propagation Conditions for Static Multipath Fading Environment

Tap	Relative Phases	Relative Delay (chips)	Relative Power (dB)
1	0^{o}	0	0.0
2	60^{o}	1	-1.5
3	120^{o}	2	-3.0
4	180^{o}	3	-4.5

In the simulation, the channel coefficients are normalized to give unity power gain. The power delay profile of this channel is displayed in Figure 14.

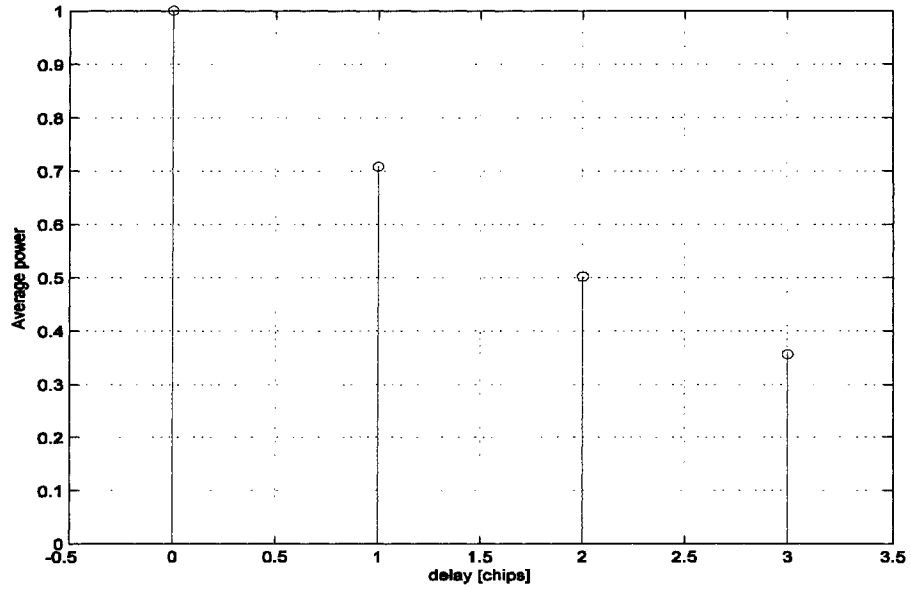

Figure 14: Fixed Coefficients Channel – Power Delay Profile

5.2.2 Time-Variant Channels

In this section, three separate multipath fading channel models that are used to evaluate the performance of the G-RAKE receiver are presented. In modeling the realistic time-dispersive properties of the channels, classical Doppler spectrum is used [15]. The channel coefficients are Rayleigh distributed and their phases are uniformly distributed between 0 and 2π. They are normalized to give unity power gain.

The chip period, T_c, is approximately 260 ns for the chip rate of 3.84 Mcps. Using the value of T_c, the multipath delay for each ray is calculated in number of chips.

For a given vehicular speed v, the maximum and normalized Doppler frequencies are evaluated using Eq A.24 and Eq A.25 given in the Appendix A.

Table 6 shows the propagation conditions that are used for the performance measurements in Case 3 channel model given in [24] for the vehicular test environment.

The vehicular speed is assumed to be 120 km/h for this case. The power delay profile of this channel is displayed in Figure 15.

Table 6: Propagation Conditions for Time-varying Multipath Fading Environment: Case 3

Tap	Relative Delay (ns)	Relative Delay (chips)	Relative Mean Power (dB)
1	0	0	0.0
2	260	1	-3.0
3	521	2	-6.0
4	781	3	-9.0

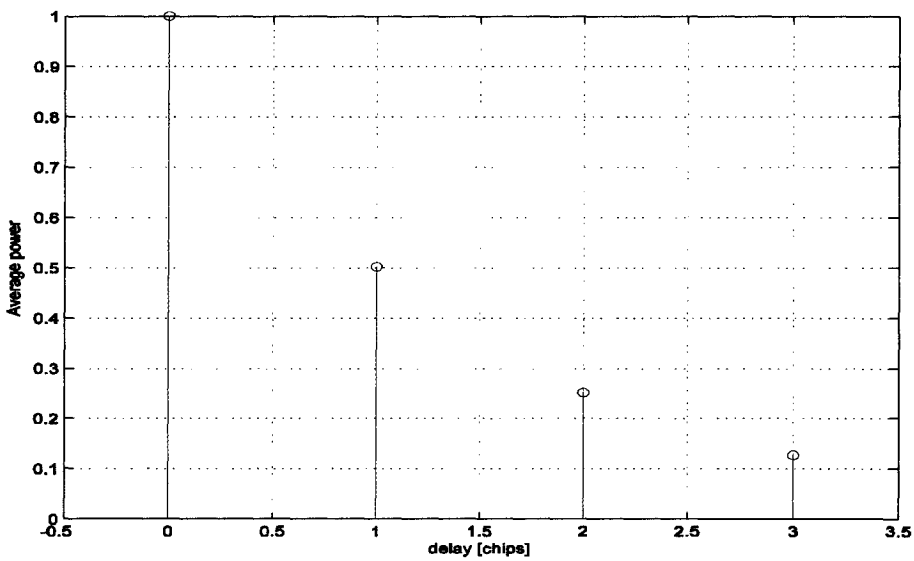

Figure 15: Case 3 Multipath Fading Channel – Power Delay Profile

Table 7 shows the propagation conditions that are used for the performance measurements in ITU classical channel model A given in [15] for the vehicular test environment. Also, this channel model is classified in [24] for HSDPA performance measurements in multipath fading environment. The vehicular speed is assumed to be 120 km/h for this channel.

Table 7: Propagation Conditions for ITU Vehicular Channel A

Tap	Relative Delay (ns)	Actual Relative Delay (chips)	Modified Relative Delay (chips)	Relative Mean Power (dB)
1	0	0	0	0.0
2	310	1.19	1	-1.0
3	710	2.73	3	-9.0
4	1090	4.19	4	-10.0
5	1730	6.64	7	-15.0
6	2510	9.64	10	-20.0

The above channel is modified to have relative delays that are integer multiples of the chip duration in order to make the simulation less complex. In Table 7, the actual relative delays are rounded up to the nearest integer and tabulated in column 4. The average power delay profile for the modified version of this channel is displayed in Figure 16.

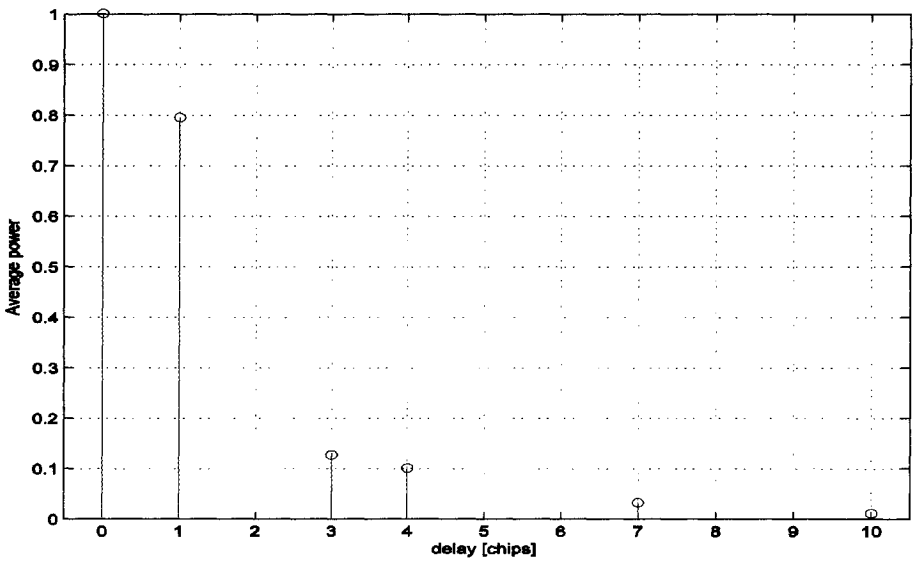

Figure 16: ITU Vehicular Channel A – Power Delay Profile

Table 8 shows the propagation conditions that are used for the performance measurements in ITU classical channel model B given in [15] for the pedestrian test environment. This channel model is classified in [24] for HSDPA performance

measurements in multipath fading environment as well. The pedestrian speed is assumed to be 3 km/h for this channel.

Table 8: Propagation Conditions for ITU Pedestrian Channel B

Tap	Relative Delay (ns)	Actual Relative Delay (chips)	Modified Relative Delay (chips)	Relative Mean Power (dB)
1	0	0	0	0.0
2	200	0.77	1	-0.9
3	800	3.08	3	-4.9
4	1200	4.62	5	-8.0
5	2300	8.85	9	-7.8
6	3700	14.23	14	-23.9

As is done for the ITU Vehicular Channel A, the actual relative delays are rounded up to the nearest integer and tabulated in column 4 for this channel as well. The average power delay profile for the modified version of this channel is displayed in Figure 17.

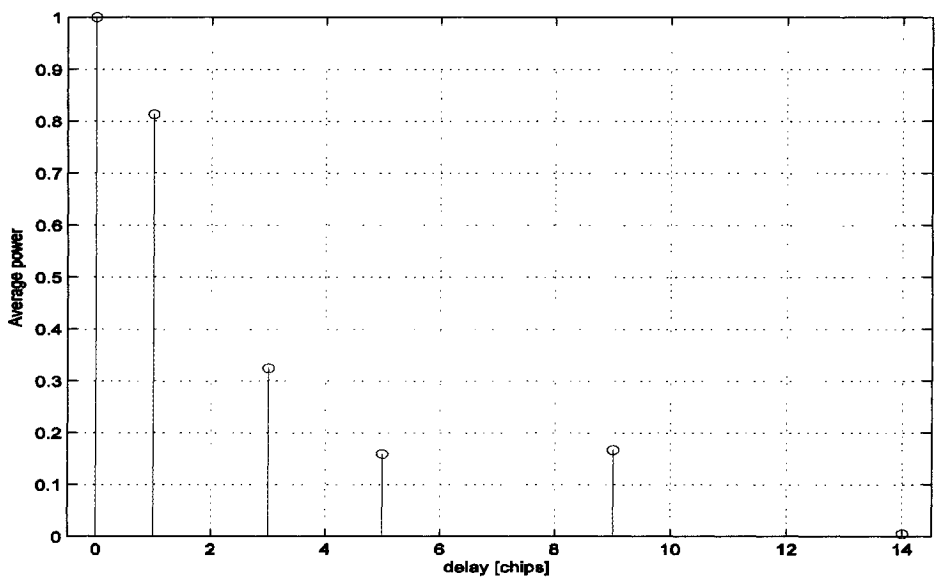

Figure 17: ITU Pedestrian Channel B – Power Delay Profile

5.3 Simulation Results

The performance results obtained through simulation are presented and discussed in this section. It should be noted that these results are obtained without channel coding.

When coding is included, the bit error rates will be much lower [25]. For example, uncoded BER in the range of 10^{-1} to 10^{-2} may reduce to 10^{-3} to 10^{-4} range with coding.

5.3.1 Performance over Time-Invariant Channel

This section captures the G-RAKE performance results for the static fading channel introduced in section 5.2.1.

One of the BER performance results presented in [4] is reproduced in Figure 18 for completeness and to validate the simulation model in this thesis. All curves but GRAKE[-1 0 1] can be found in [4]. The simulation is performed using the parameters summarized in the following table.

Modulation	Uncoded Data Rate	Spreading Factor	Number of Users
QPSK	1.44 Mbit/s	128	24

For the RAKE receiver, the fingers are placed at 0, 1, 2, and 3 chip periods corresponding to the multipath delays. Placing the fingers at these same locations for the G-RAKE offers performance gain. Such gain is due to the fact that the G-RAKE treats the MUI/MCI as correlated noise whereas RAKE considers them as uncorrelated.

When three fingers are placed at –1, 0, and 1 chip periods as shown by the curve GRAKE[-1 0 1], the performance improves significantly. In fact, the total energy collected for all available multipath components is reduced in this scenario. Nonetheless, placing a finger just before the strongest multipath contributes to canceling the correlated noise.

Placing the fingers at -1, 0, 1, and 2 chip periods by adding one more finger to the above scenario, shown by the curve GRAKE[-1 0 1 2], improves the performance slightly further. This finger combination produces higher output SNR compared to the previous combination and, thus, contributes to improving the performance.

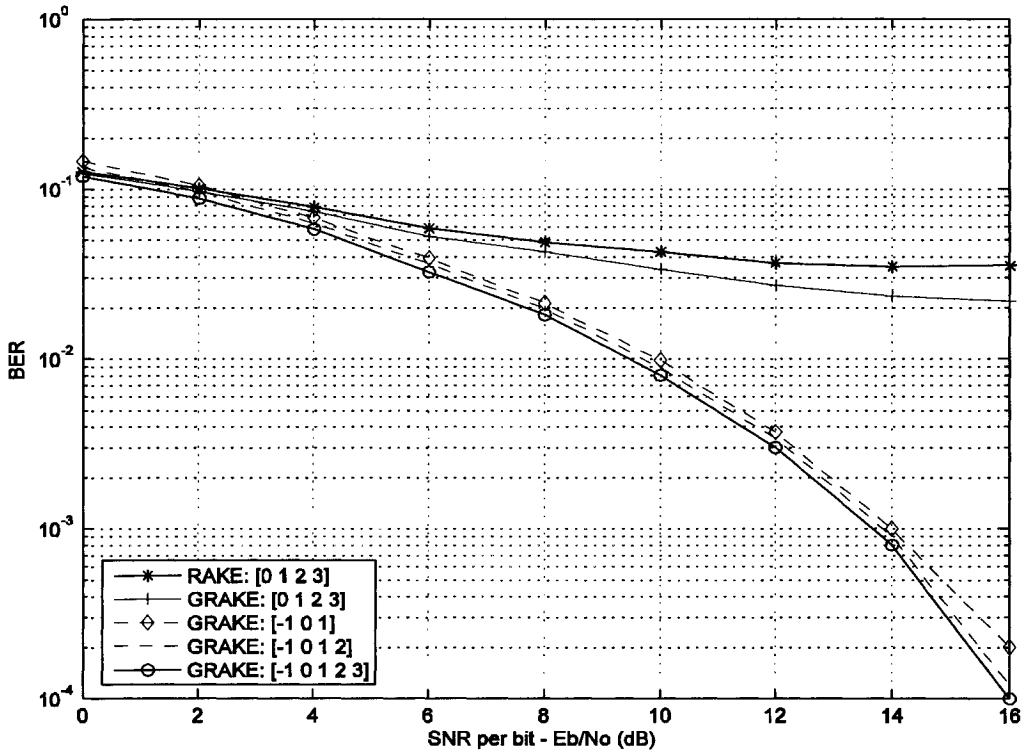

Figure 18: RAKE and G-RAKE performance. Modulation is QPSK. SF=128. Number of Users = 24. The channel is static and has four chip-spaced paths with relative power 0.0, -1.5, -3.0, and -4.5 dB, and relative phases 0°, 60°, 120°, and 180°. All curves but GRAKE[-1 0 1] are reproduced from [4]

The GRAKE[-1 0 1 2 3] curve is for fingers placed at -1, 0, 1, 2, and 3 chip periods. For this finger combination, the performance dramatically improves because the extra finger at the location before the strongest path partially eliminates the overall interference. This tells us that there is correlation between the noise present on this extra finger and the noise present on all other four fingers, leading to partial cancellation of the overall interference.

Consequently, the G-RAKE receiver outperforms the RAKE receiver in this fading environment as it partially cancels the overall correlated noise in the fingers placed at multipath locations. The decision over the total number of fingers to use in the G-RAKE receiver depends on how much performance degradation can be tolerated by reducing the total energy collected.

The performance results obtained for the simulation parameters in the following table are given in Figure 19.

Modulation	Uncoded Data Rate	Spreading Factor	Number of Users
16-QAM	1.92 Mbit/s	16	2

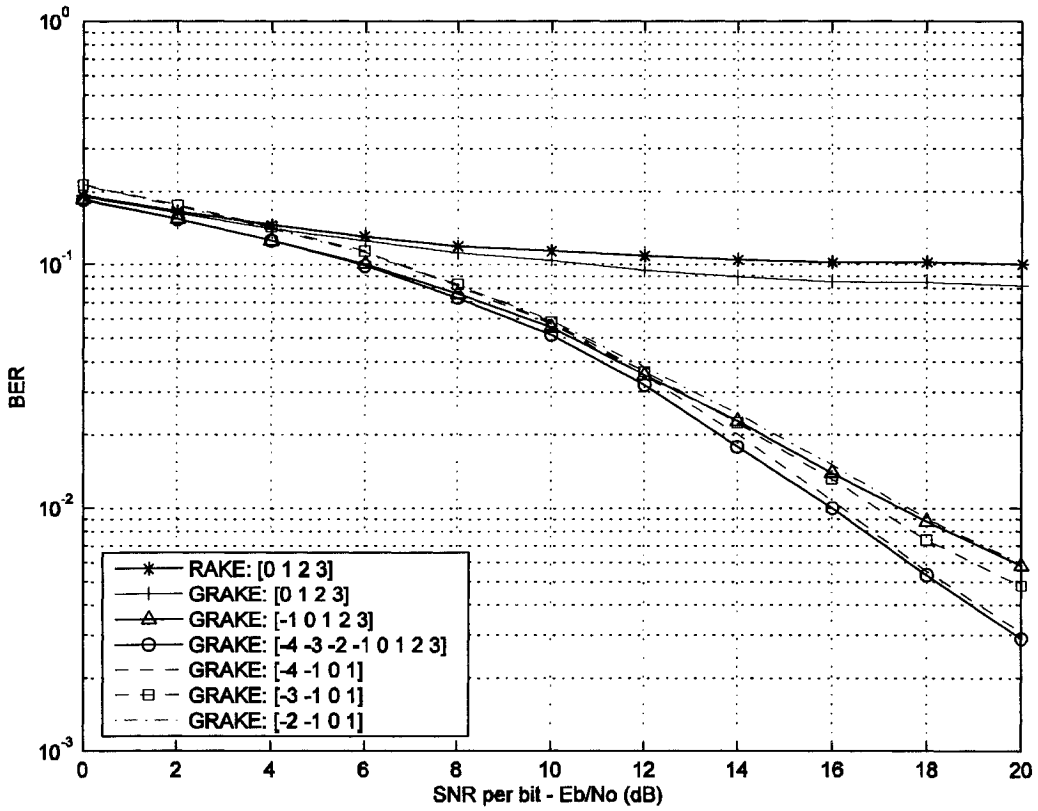

Figure 19: RAKE and G-RAKE performance. Modulation is 16-QAM. SF = 16. Numer of users = 2. The channel is static and has four chip-spaced paths with relative power 0.0, -1.5, -3.0, and -4.5 dB, and relative phases 0°, 60°, 120°, and 180°.

The curve for RAKE[0 1 2 3] depicts the effect of placing four fingers at 0, 1, 2, and 3 chip periods for the RAKE receiver. As can be seen, its performance is very poor as it fails to suppress the interference noise.

When the channel is matched by placing fingers at the multipaths 0, 1, 2, and 3 chip periods for the G-RAKE receiver, the performance improves as shown by the curve GRAKE[0 1 2 3].

The curve GRAKE[-1 0 1 2 3] shows the placement of five fingers at -1, 0, 1, 2, and 3 chip periods for the G-RAKE receiver. Significant performance gain over the RAKE is obtained by adding an extra finger just before the strongest multipath component. Again, this additional finger contributes to canceling the correlated noise present in the system and, thereby, increasing the output SNR of the G-RAKE receiver.

The curve GRAKE[-4 -1 0 1] is the effect of having four fingers at -4, -1, 0, and 1 chip periods. Similarly, the curve GRAKE[-3 -1 0 1] is the result of placing fingers at -3, -1, 0, and 1 chip periods. In both cases, fingers are placed only at the first two strongest multipaths in addition to assigning two extra fingers before the strongest multipath component. Both curves demonstrate the tradeoff between collecting signal energy and canceling the correlated noise. However, it is interesting to notice that the performance of GRAKE[-4 -1 0 1] is better than that of G-RAKE[-3 -1 0 1]. This tells us that by placing those two extra fingers at -4 and -1 chip periods instead of at -3 and -1 chip periods, the correlated noise is cancelled more and higher output SNR is produced.

Although it is not shown in the figure, adding fingers to the G-RAKE receiver at -3 chip period as depicted in the curve GRAKE[-3 -1 0 1 2 3] produces almost the same performance as the curve GRAKE[-3 -1 0 1].

It is observed that the performance curves GRAKE[-2 -1 0 1] and GRAKE[-1 0 1 2 3] almost follow each other. As these two finger combinations give almost equal output SNR, their performance tends to match each other. These curves demonstrate that significant gain can be achieved by just having the same number of fingers as the number of multipath components for the G-RAKE receiver.

The curve GRAKE[-4 -3 -2 -1 0 1 2 3] is the result of employing eight fingers in total, each placed at -4, -3, -2, -1, 0, 1, 2, and 3 chip periods. From the series of curves, it is noticeable that adding twice as many fingers as the number of multipath components gives better BER performance. This combination gives slightly better performance than that of GRAKE[-4 -1 0 1]. Again, this demonstrates the trade-off between the number of fingers and the performance gain; that is, smaller number of fingers can also give comparable performance gain.

In Figure 20, the BER performance curves obtained for the simulation parameters in the following table are plotted.

Modulation	Uncoded Data Rate	Spreading Factor	Number of Users
16-QAM	7.68 Mbit/s	16	8

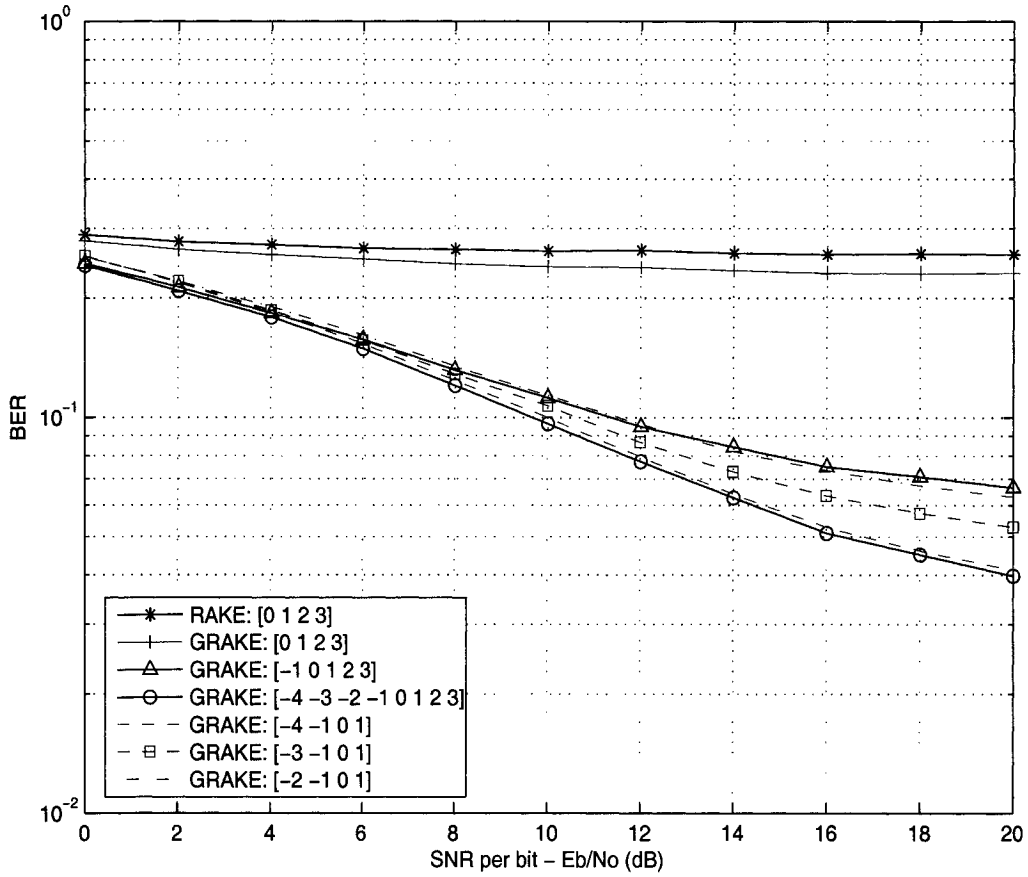

Figure 20: RAKE and G-RAKE performance. Modulation is 16-QAM. SF = 16. Number of users = 8. The channel is static and has four chip-spaced paths with relative power 0.0, -1.5, -3.0, and -4.5 dB, and relative phases 0°, 60°, 120°, and 180°.

Similar arguments as for the simulation result in Figure 19 hold true for this scenario. Overall, the G-RAKE receiver outperforms the RAKE receiver. However, as the number of users/codes utilized here is higher, the MUI/MCI increases. This in effect degrades the performance and raises the BER.

In Figure 21, the BER performance curves obtained for the simulation parameters in the following table are presented.

Modulation	Uncoded Data Rate	Spreading Factor	Number of Users
16-QAM	14.4 Mbit/s	16	15

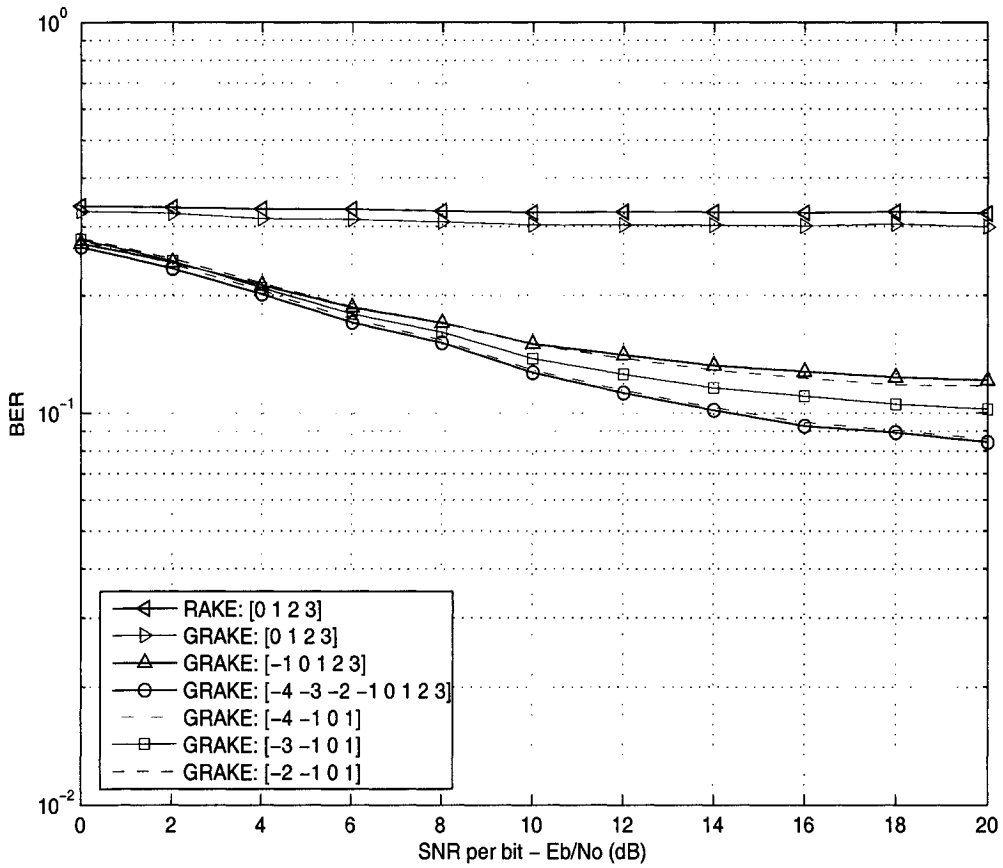

Figure 21: RAKE and G-RAKE performance. Modulation is 16-QAM. SF = 16. Number of users = 15. The channel is static and has four chip-spaced paths with relative power 0.0, -1.5, -3.0, and -4.5 dB, and relative phases 0°, 60°, 120°, and 180°.

Again, similar arguments as for the simulation result in Figure 19 hold true for this scenario as well. However, as the number of users/codes reaches the available maximum (i.e. 15 shared codes), the MUI/MCI amounts higher. Consequently, the performance of

G-RAKE deteriorates even when having twice as many fingers as the number of multipath components. Although the G-RAKE receiver outperforms the RAKE receiver, the system becomes more interference limited with increased number of users. The BER is in the order of 10^{-1} for high SNR and higher for low SNR. This does not seem an acceptable error level for a fully loaded HSDPA with 16-QAM modulation.

Three performance results are presented above for the 16-QAM modulation with increasing number of users/codes. In all three results, it is shown that G-RAKE receiver fingers can be chosen to give significant performance gain over the conventional RAKE receiver based on the output SNR at the G-RAKE receiver. By comparing the G-RAKE performance with the number of users, it can be concluded that the performance worsens as the number of users/codes increases since the system becomes more interference limited.

5.3.2 Performance over Time-Variant Channels

This section captures the G-RAKE performance results for the realistic multipath fading channels introduced earlier in section 5.2.2.

The following parameters are kept constant in the simulation for each time-variant channel.

Modulation	Uncoded Data Rate	Spreading Factor	Number of Users
16-QAM	7.68 Mbit/s	16	8

The BER performance of the G-RAKE receiver for the channel in Table 6 is captured in Figure 22.

The effect of placing four fingers at 0, 1, 2, and 3 chip periods for the RAKE receiver, corresponding to each multipath component, is represented by RAKE[0 1 2 3]. As the correlated noise is not removed by the RAKE, there exists an error floor.

As observed in previous results, allocating fingers at locations correspond to the multipath components for the G-RAKE receiver shows considerable performance improvement. This is shown by the curve GRAKE[0 1 2 3].

As expected, the GRAKE[-1 0 1 2] yields some performance gain over the GRAKE[0 1 2 3], albeit small. The finger placed just before the strongest multipath tends to partially cancel the interference present in the system.

When the channel is fully matched and an extra finger is placed just before the strongest multipath component as shown by the curve GRAKE[-1 0 1 2 3], the performance improves further. The GRAKE[-2 -1 0 1 2 3] shows the curve for assigning fingers at -2, -1, 0, 1, 2, and 3 chip periods for the G-RAKE receiver. This shows significant improvement in performance over the RAKE as the fingers at -2 and -1 chip periods together play the role of canceling the correlated noise present in the system. This finger

combination performs better than the GRAKE[-4 -3 -2 -1 0 1 2], which represents the performance obtained for fingers placed at -4, -3, -2, -1, 0, 1, and 2 chip periods. As seen in previous results, this demonstrates the trade-off between canceling the interference and matching the channel (collecting energy).

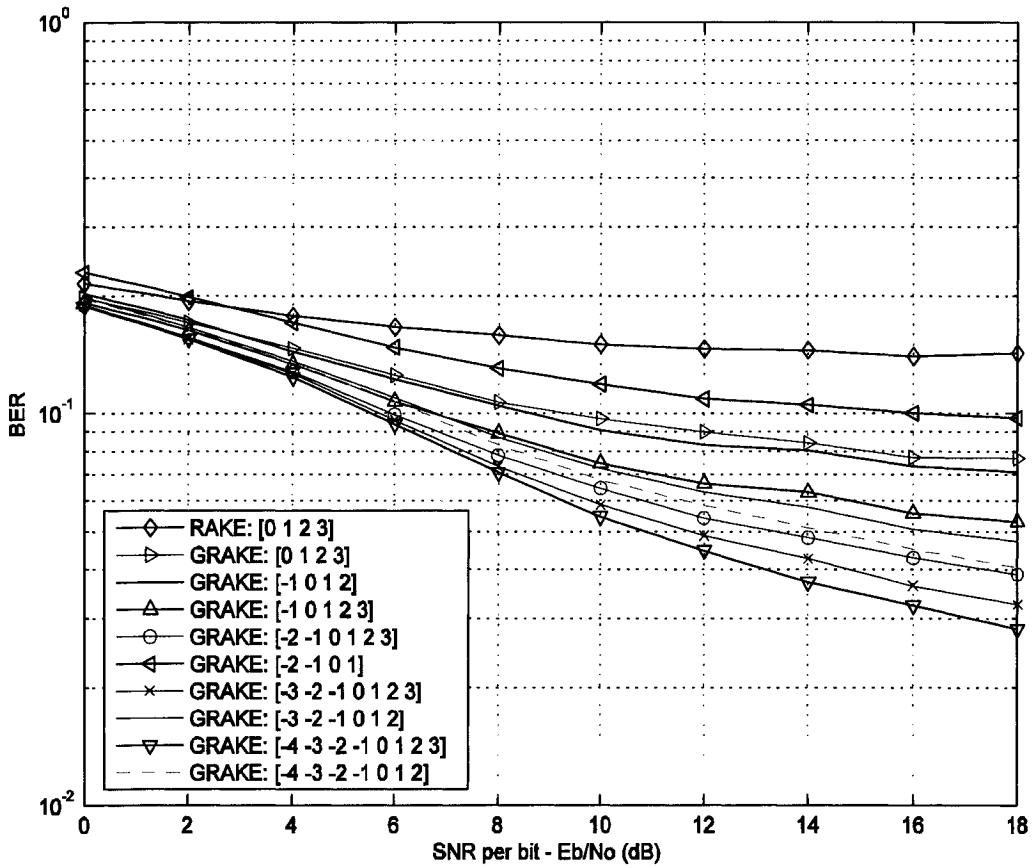

Figure 22: RAKE and G-RAKE Performance. Modulation is 16-QAM. SF = 16. Mobile Speed = 120 km/h. Number of Users = 8. The multipath fading channel is the Case 3 channel that has 4 chip-spaced rays with average power 0.0, -3.0, -6.0, and –9.0 dB.

Allocation of additional fingers before the strongest multipath at locations –2, -3, and –4 results in improved performance as observed by the curves GRAKE[-2 –1 0 1 2 3], GRAKE[-3 –2 –1 0 1 2 3], and GRAKE[-4 –3 –2 –1 0 1 2 3] . As can be seen from the GRAKE[-4 -3 -2 -1 0 1 2 3] curve, allocating eight fingers at -4, -3, -2, -1, 0, 1, 2, and 3 chip periods gives superior performance. This is in line with the nominal value of fingers

of choice given in the literature; that is, the number of fingers is twice as many as the number of fading rays. Also, this combination produces maximum SNR (average) at the receiver output.

Noticeably, the performance of GRAKE[-2 -1 0 1] is worse than the GRAKE[0 1 2 3] for this channel. This is in contrast to the performance behaviour observed for the time-invariant channel earlier in which the GRAKE[-2 -1 0 1] performed much better than the GRAKE[0 1 2 3]. It can be claimed that this difference is well due to the channel conditions.

Overall, the results show that the G-RAKE receiver can substantially improve the BER performance over the RAKE receiver in a typical time-varying frequency fading channel conditions in the downlink. Of the chosen finger combinations, the best combination of fingers that yields in the maximum SNR is found to have performed better than others.

Next, the performance of G-RAKE receiver for the ITU Vehicular channel A in Table 7 is captured in Figure 23.

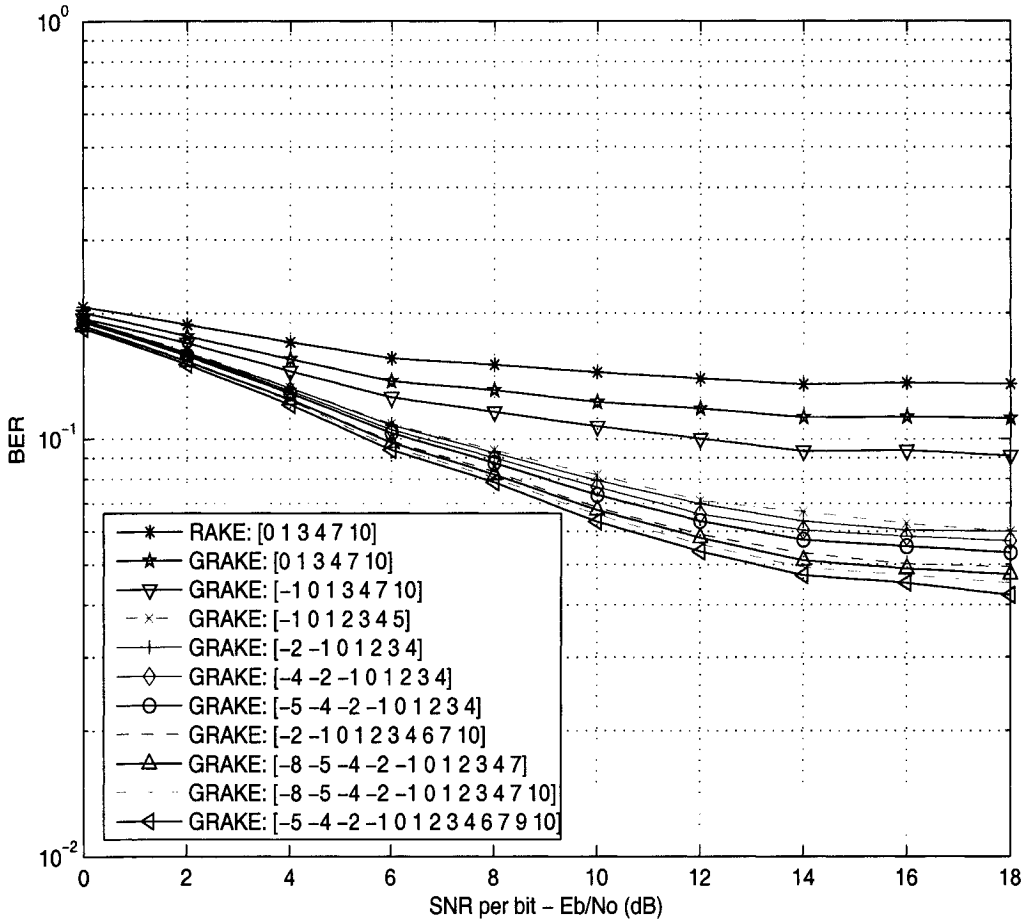

Figure 23: RAKE and G-RAKE Performance. Modulation is 16-QAM. SF = 16. Mobile Speed = 120 km/h. Number of Users = 8. The multipath fading channel is the ITU Vehicular channel A that has 6 rays at chip periods 0, 1, 3, 4, 7, and 10 with average power 0.0, -1.0, -9.0, 10.0, -15.0, and –20.0 dB.

The effect of placing six fingers at 0, 1, 3, 4, 7, and 10 chip periods for the RAKE receiver, corresponding to each multipath component, is represented by RAKE[0 1 3 4 7 10]. An error floor is observed when RAKE matches the channel as it handles the interference present in the system as white.

As observed in previous results, allocating fingers at locations correspond to the multipath components for the G-RAKE receiver shows considerable performance improvement. This is shown by the curve GRAKE[0 1 3 4 7 10].

The performance curve GRAKE[-1 0 1 3 4 7 10] obtained by placing fingers at -1, 0, 1, 3, 4, 7, and 10 chip periods is better than the performance seen for GRAKE[0 1 3 4 7 10]. As found in previous results, the additional finger placed just before the strongest multipath component partially cancels the overall correlated noise present in the system and, thus, leads to the performance gain.

The rest of the curves in the figure show G-RAKE performance with different combinations of fingers. It is noticed that a finger combination that performs better than another in terms of minimum BER also produces higher output SNR. When twelve fingers are allocated at -8, -5, -4, -2, -1, 0, 1, 2, 3, 4, 7, and 10 chip periods, the performance observed is quite better. Again, this is in line with the nominal number of fingers of choice found in the literature. Of all the finger combinations chosen, the G-RAKE[-5 -4 -2 -1 0 1 2 3 4 6 7 9 10] curve, allocating thirteen fingers at -5, -4, -2, -1, 0, 1, 2, 3, 4, 6, 7, 9 and 10 chip periods gives superior performance. This combination contains more than twice as many fingers as the number of fading rays. It demonstrates that further addition of fingers can buy some performance gain, albeit small. Also, this combination produces maximum SNR (average) at the receiver output.

The results show the merits of the G-RAKE receiver that can improve the BER performance over the RAKE receiver in a realistic time-varying frequency-selective fading channel in vehicular test environment for the downlink.

Finally, to capture the performance of the G-RAKE receiver in a realistic pedestrian fading channel conditions, the ITU Pedestrian channel B in Table 8 is used and the results are presented in Figure 24.

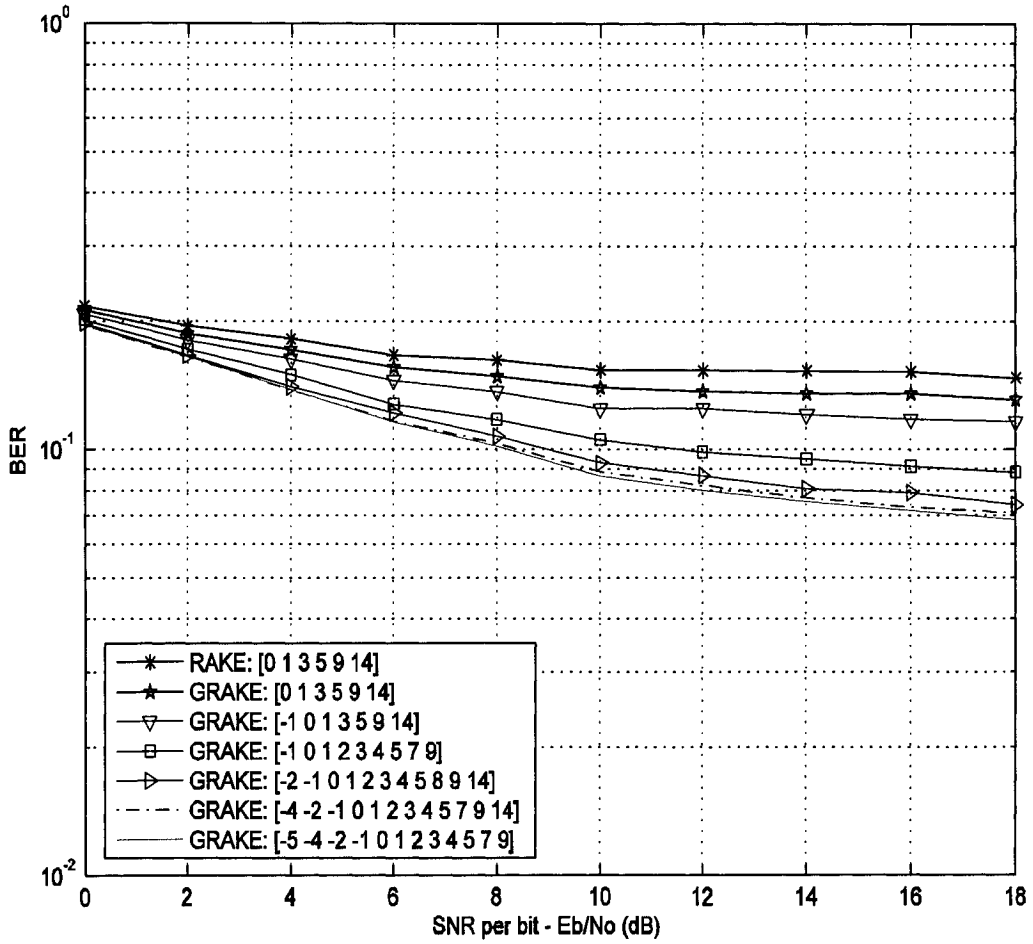

Figure 24: RAKE and G-RAKE Performance. Modulation is 16-QAM. SF = 16. Mobile Speed = 120 km/h. Number of Users = 8. The multipath fading channel is the ITU Pedestrian channel B that has 6 rays at chip periods 0, 1, 3, 5, 9, and 14 with average power 0.0, -0.9, -4.9, 8.0, -7.8, and –23.9 dB.

Similar arguments as for the previous result in Figure 23 can be made to the performance behaviour of the G-RAKE receiver over the RAKE in this channel condition as well.

Although it is not shown in the figure, the performance of GRAKE[-4 –2 –1 0 1 2 3 4 5 8 9 14], GRAKE[-2 –1 0 1 2 3 4 5 8 9 14], GRAKE[-2 –1 0 1 2 3 4 5 8 9 12 14], and

GRAKE[-4 -2 -1 0 1 2 3 4 5 7 9 12] are found to have performed very closer to the performance shown by the curve GRAKE[-4 –2 –1 0 1 2 3 4 5 7 9 14].

Of all the finger combinations chosen, allocating twelve fingers at -5, -4, -2, -1, 0, 1, 2, 3, 4, 5, 7, and 9 chip periods, shown by the curve GRAKE[-5 -4 -2 -1 0 1 2 3 4 5 7 9], gives superior performance. Again, this is in line with the nominal value of fingers of choice given in the literature. Also, this combination among others produces maximum SNR (average) at the receiver output.

Once again, this exhibits the intrinsic worth of the G-RAKE receiver over the RAKE receiver in a realistic time-varying frequency-fading channel conditions in the downlink. The G-RAKE receiver outperforms the RAKE by providing a mechanism to cancel the interference (correlated noise) present in the system.

5.3.3 Convergence Behaviour of Iterative Methods

This section examines the iterative methods detailed in chapter 4 to calculate the weighting coefficients for the G-RAKE combining. The channel used in these simulations is the chip-spaced static multipath channel described in section 5.2.1. The convergence behaviour of each iterative method is studied using the simulation parameters in the following table.

Modulation	Uncoded Data Rate	Spreading Factor	Number of Users
16-QAM	7.68 Mbit/s	16	8

5.3.3.1 Gauss-Seidel (GS) Method

In Figure 25, the BER performance for the G-RAKE receiver with the use of GS method to iteratively compute the combining weights is shown. This method converges to the desired

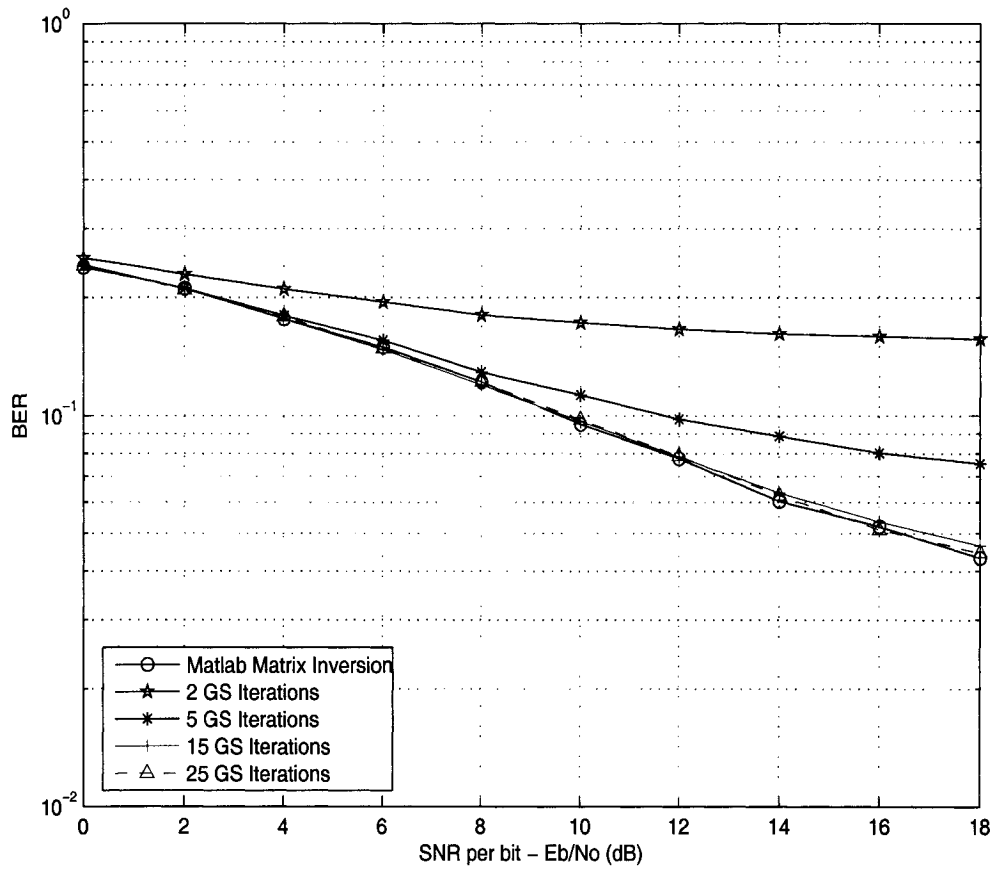

Figure 25: G-RAKE performance for 16-QAM modulation with 8 users. The channel is static and has four chip-spaced paths with relative power 0.0, -1.5, -3, and -4.5 dB, and relative phases 0°, 60°, 120°, and 180°. Gauss-Seidel Iterative and Matlab's Matrix Inversion methods are used.

solution in 15-25 iterations. In the literature [26], it is reported that this method should converge within 3 iterations. As the below shown covariance matrix, $\mathbf{R}_u$, which is generated for this channel, has mild diagonal dominance (at least one diagonal element of the matrix satisfies Eq 4.2, but not all diagonal elements), the convergence takes more iterations.

$$\begin{bmatrix}
1.93 & 0.66-j1.56 & -0.43-j0.74 & -0.42 & 0 & 0 & 0 & 0 \\
0.66+j1.56 & 1.91 & 0.66-j1.14 & -0.43-j0.74 & -0.42 & 0 & 0 & 0 \\
-0.43+j0.74 & 0.66+j1.14 & 1.90 & 0.65-j1.13 & -0.42-j0.73 & -0.41 & 0 & 0 \\
-0.42 & -0.43+j0.74 & 0.65+j1.13 & 1.88 & 0.64-j1.12 & -0.42-j0.72 & 0.41 & 0 \\
0 & -0.42 & -0.42+j0.73 & 0.64+j1.12 & 1.18 & 0.35-j0.61 & 0.17-j0.30 & 0 \\
0 & 0 & -0.41 & -0.42+j0.72 & 0.35+j0.61 & 1.38 & 0.44-j0.75 & -0.24-j0.42 \\
0 & 0 & 0 & -0.41 & -0.17+j0.30 & 0.44+j0.75 & 1.53 & 0.50-j0.86 \\
0 & 0 & 0 & 0 & 0 & -0.24+j0.42 & 0.50+j0.86 & 1.64
\end{bmatrix}$$

It is possible that the diagonal dominance is influenced by the type of multipath channel and the modulation scheme used.

5.3.3.2 Successive Over-relaxation (SOR) Method

The convergence behaviour of the SOR method is studied for arbitrarily chosen values of the relaxation parameter ω. The number of iterations taken for the method to converge to the exact solution is tabulated in Table 9.

Table 9: SOR Iterations for Different Values of Relaxation Parameter

Relaxation Parameter ω	Number of Iterations
0.7	> 20
0.8	16-17
0.9	15-16
1.0	24-25
1.1	14-15
1.2	12-13
1.25	12-13
1.3	12-13
1.35	11-12
1.40	11-12
1.45	12-13
1.7	20-21
1.85	> 40

Faster convergence to the exact solution is achieved when ω ranges between 1.25 and 1.55. The behaviour that converges to the exact solution when ω =1.25 is shown in Figure 26.

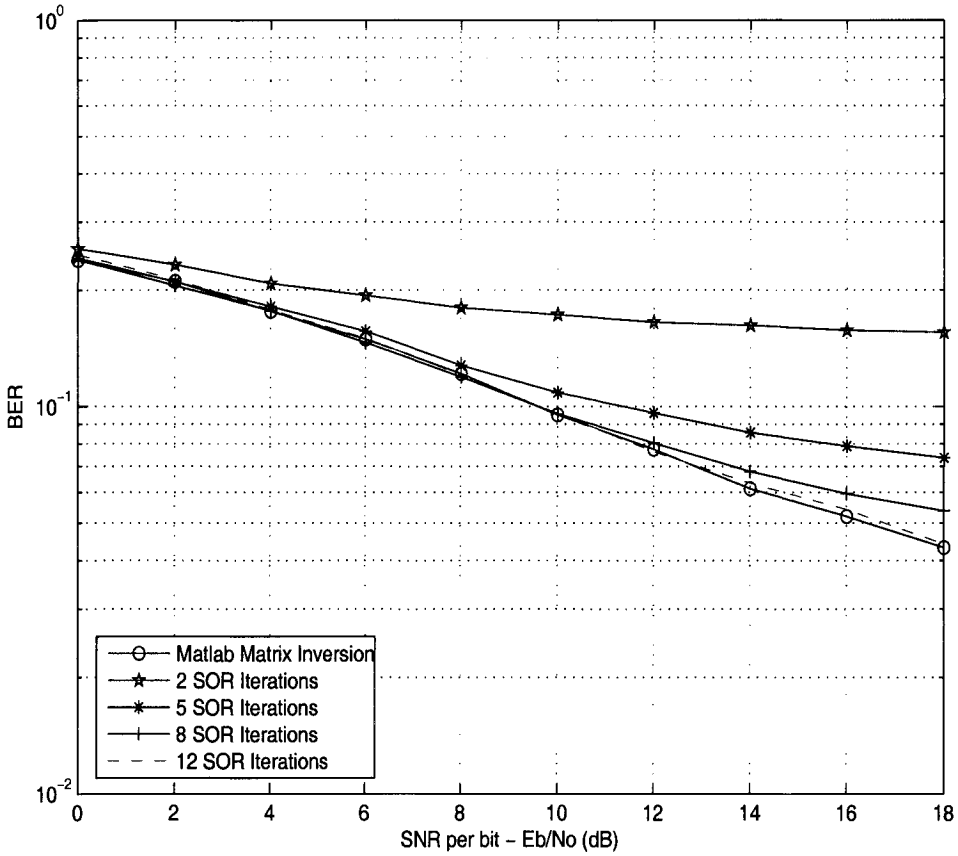

Figure 26: G-RAKE performance for 16-QAM modulation with 8 users. The channel has four chip-spaced paths with relative power 0.0, -1.5, -3.0, and -4.5 dB, and relative phases 0°, 60°, 120°, and 180°. SOR and Matlab's Matrix Inversion methods are used.

This method converges to the direct solution with 12 iterations. Even though the SOR method performs better than the GS in terms of the number of iterations, the number is still bigger.

5.3.3.3 Conjugate Gradient (CG) Method

The BER performance for the G-RAKE receiver with the use of CG method to iteratively calculate the combining weights is illustrated in Figure 27. This method converges to the desired solution in 5-10 iterations, which conforms to the theoretically expected number of iterations.

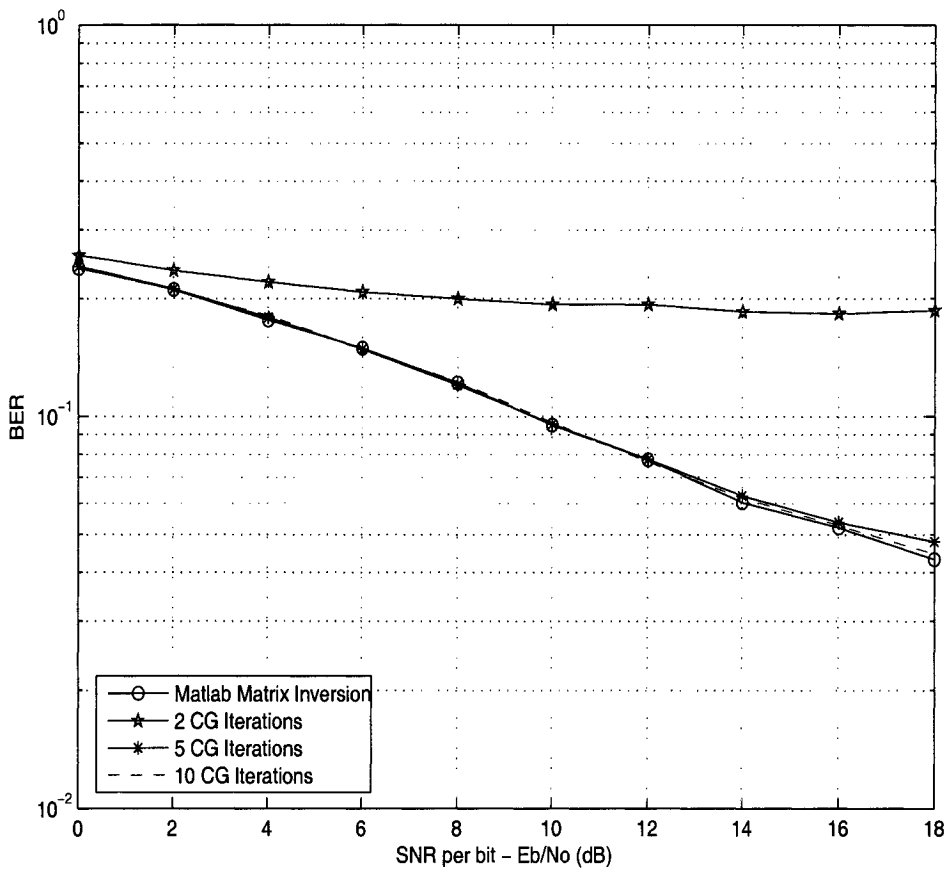

Figure 27: G-RAKE performance for 16-QAM modulation with 8 users. The channel has four chip-spaced paths with relative power 0.0, -1.5, -3.0, and -4.5 dB, and relative phases 0°, 60°, 120°, and 180°. Conjugate Gradient and Matlab's Matrix Inversion methods are used.

In comparison, the classical CG method is more than 3 times faster than the GS method. The reason for this is that the CG method does not have any dependency on the diagonal dominance of the covariance matrix. As long as the covariance matrix is positive-definite, the CG method converges within reasonable number of iterations.

5.3.3.4 Preconditioned Conjugate Gradient (PCG) Method

The BER performance for the G-RAKE with the use of PCG method to iteratively determine the combining weights is illustrated in Figure 28.

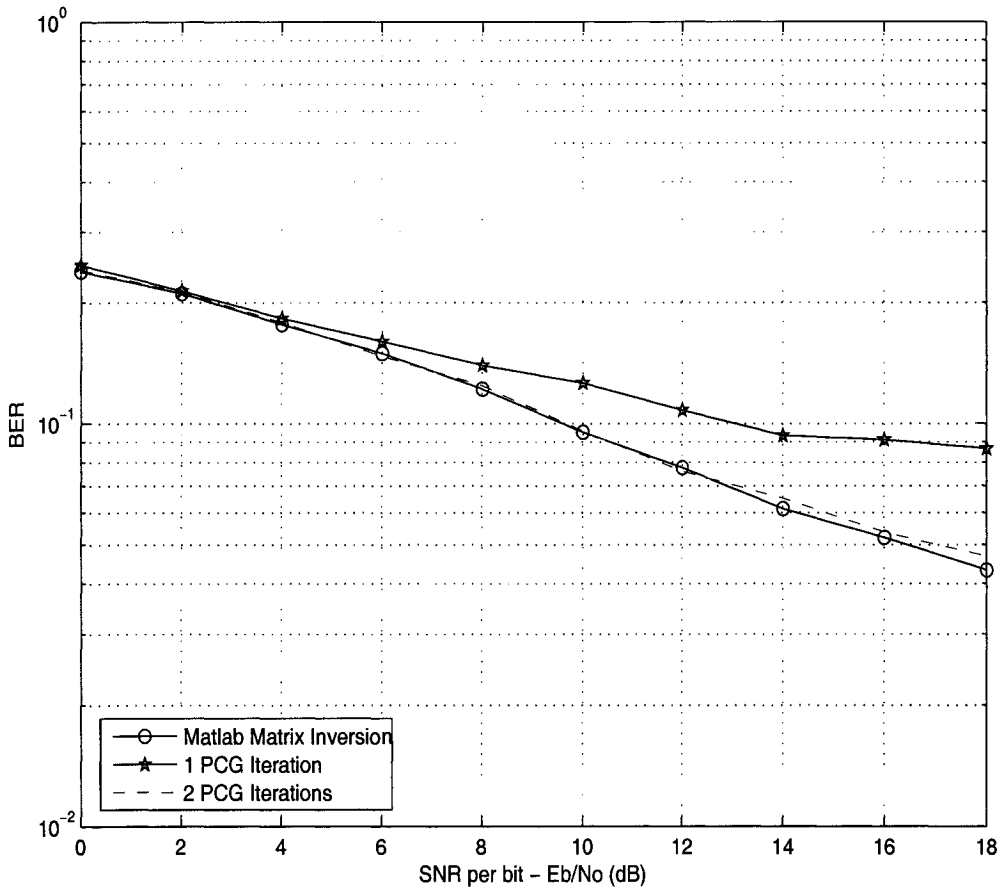

Figure 28: G-RAKE performance for 16-QAM modulation with 8 users. The channel has four chip-spaced paths with relative power 0.0, -1.5, -3.0, and -4.5 dB, and relative phases 0°, 60°, 120°, and 180°. PCG and Matlab's Matrix Inversion methods are used.

The SSOR-PCG method converges to the desired solution in 2 iterations. This is an expected result over the CG method as preconditioning reduces the condition number of the covariance matrix and, thus, accelerates convergence.

In comparison to the GS method, the PCG is much better in terms of the number of iterations taken to compute the combining weights of the G-RAKE receiver as it does not rely on the diagonal dominance of the covariance matrix, but on the type of preconditioner being used.

CHAPTER 6

6. Conclusion

6.1 Summary of the Results

In this thesis, the performances of the RAKE and G-RAKE receivers are evaluated in both static and time-varying multipath fading channels for HSDPA applications (high speed data rate) in a single cell scenario. For the G-RAKE receiver, fingers are placed at delays that yield relatively higher SNR output (averaged over the channel fading coefficients) at the receiver as suggested in [4].

It is shown in the simulations that the performance of the RAKE receiver is heavily limited by the interference (coloured noise) present in its fingers' output and, therefore, cannot be used in systems that are meant for higher data rates such as HSDPA. As the simulation results indicate, the performance gain is substantial when the G-RAKE receiver replaces RAKE receiver as it handles the interference present in the system as coloured. For all fading channels used, it is shown that matching the channel by allocating G-RAKE fingers at the resolvable multipath components could obtain significant performance gain over the RAKE receiver. The performance of the G-RAKE gets better as the number of fingers reaches twice as many as the number of multipath components. Also, it is found that the extra finger placed just before the strongest ray plays a vital role in canceling the correlated noise present in the system. Overall, the G-RAKE receiver outperforms the RAKE receiver in both types of channels.

It is observed that the G-RAKE receiver performance with spreading factor 16 and 16-QAM modulation becomes poorer than that of with spreading factor 128 and QPSK modulation. This is because the interference due to multipaths in a cell becomes significant for low processing gain system such as HSDPA. And, this interference increases with increasing number of users, which in turn results in an error floor as the G-RAKE receiver employs the maximum number of spreading codes available. A full

system level performance analysis would reveal the actual performance behaviour of the use of G-RAKE receiver in the HSDPA scenario.

The simulations are performed without channel coding in this thesis. It can be stated that the performance of the G-RAKE receiver can be further improved with channel coding.

As far as the complexity reduction of the G-RAKE receiver is concerned, some popular iterative methods such as the Gauss-Seidel and Conjugate Gradient are shown as viable alternatives to the inversion of the covariance matrix. It is found through simulations that the Conjugate Gradient method or possibly the Preconditioned Conjugate method would be an ideal choice for inverting the covariance matrix as these methods do not rely on the diagonal dominance of the matrix. These iterative methods are computationally less complex than the direct matrix inversion method and comparable to the complexity of the Gauss-Seidel iterative method. Also, they converge much faster than the Gauss-Seidel method.

6.2 Future Research

In practice, only a moderate number of users (i.e. ~10) can occupy the band for reasonable bit error rate (BER) performance for HSDPA. Thus, the Gaussian assumption of the colored interference may not be realistic. This leads to devising a proper mathematical model for the G-RAKE in this case.

Another possible area of research involves finding an efficient finger placement strategy to improve the performance of the G-RAKE receiver. The complexity of such method should be kept to an acceptable level.

Implementing the matrix inversion techniques outlined in Chapter 4 in hardware for the G-RAKE receiver and a comparison study of the results will contribute to this area further.

Appendix A – Basic Wireless Communication Systems Concepts

The section covers some useful performance measures and concepts in digital communication systems and building blocks related to WCDMA system that may be of interest to the reader.

A.1 Additive White and Coloured Gaussian Noise

Undesired signals that tend to obscure the transmission and processing of signals in communication systems are termed noise [27]. A common form of noise is thermal noise that arises from spontaneous fluctuations of electrons in electronic devices that are internal to the system and in transmission medium. The presence of this noise in the received signal is statistically modeled as Additive **White** Gaussian Noise (AWGN) random process. It is white in the sense that its power spectral density (PSD) is independent of the operating frequency. Thus, for a zero-mean AWGN sample function, *n(t)*, the PSD is

$$P_n(f) = \frac{N_o}{2} \qquad \textbf{Eq A. 1}$$

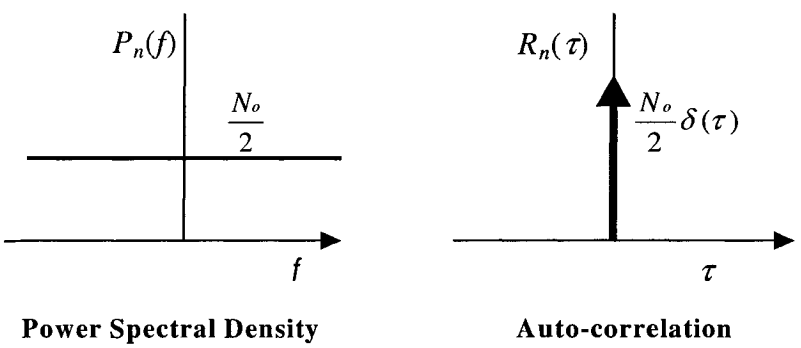

Figure 29: White Noise (i.e. AWGN)

The auto-correlation function of the AWGN noise process is given as

$$R_n(\tau) = \frac{N_o}{2}\delta(\tau) \qquad \textbf{Eq A. 2}$$

This tells us that the noise values are uncorrelated in the AWGN. The PDF of a AWGN noise vector $\mathbf{n} = [n_1, n_2, n_3, \ldots, n_m]$ denoted as $\mathbf{n} \sim N(0,\mathbf{K})$ can be mathematically written as

$$p_n(\mathbf{n}) = \frac{1}{(2\pi)^{m/2}(\det \mathbf{K})^{1/2}} e^{\left(-\frac{1}{2}\mathbf{n}^T\mathbf{K}^{-1}\mathbf{n}\right)} \qquad \textbf{Eq A. 3}$$

where $\mathbf{K}$ is the covariance matrix of $\mathbf{n}$. Thus,

$$\mathbf{K} = E[\mathbf{n}\mathbf{n}^T] = \sigma^2\mathbf{I} = \frac{N_o}{2}\mathbf{I} \qquad \textbf{Eq A. 4}$$

here $\mathbf{I}$ denotes an identity matrix and $\sigma^2 = N_o/2$ is the variance of the noise samples.

If the noise present in the received signal is non-white, it is called **coloured** noise. The PSD of the coloured noise will not be flat, and the auto-correlation of the noise process will possibly have multiple impulses. In this case, the covariance matrix is non-trivial.

In a radio communication system (e.g. WCDMA), the bandlimited version of the WGN can be regarded as the Coloured Gaussian Noise (CGN). In a WCDMA system, for instance, this band limitation facilitates the existence of both noise and interference from other users only in the frequency band of operation.

$$c(t) = n(t) * p(t) \qquad \textbf{Eq A. 5}$$

The above convolution operation illustrates a simple way of generating CGN, *c(t)*, by filtering the WGN, *n(t)*, with a signal, *p(t)*, which characterizes the interference system (i.e. bandwidth, carrier frequency).

A.2 Signal-to-Noise-Ratio

The signal-to-noise ratio (SNR) is a system parameter that accounts for the effect of noise quantitatively. In other words, it is a measure of the signal strength relative to background noise. The SNR is defined as the ratio of the average signal power to the average noise power in the signal bandwidth, both being measured at the same point. It is customarily measured in decibels (dB). Thus,

$$\text{SNR} = \frac{S}{N} \qquad \textbf{Eq A. 6}$$

where S and N are input and noise powers in watts respectively.

For an AWGN channel, suppose N_o is the power spectral density (watts/Hz) measured at the front end of the receiver and E_b is the average energy per information bit, the signal-to-noise ratio per bit is defined as

$$\text{SNR}_{[bit]} = \gamma_b = \frac{E_b}{N_o} \qquad \textbf{Eq A. 7}$$

Likewise, the signal-to-noise ratio per information symbol is defined as

$$\text{SNR}_{[sym]} = \gamma_s = \frac{E_s}{N_o} \qquad \textbf{Eq A. 8}$$

The relationship between $\text{SNR}_{[sym]}$ and $\text{SNR}_{[bit]}$, both expressed in dB, is given as

$$\mathrm{SNR}_{[sym]}(\mathrm{dB}) = \mathrm{SNR}_{[bit]}(\mathrm{dB}) + 10\log_{10}(k) \qquad \textbf{Eq A. 9}$$

where k is the number of information bits per symbol.

The relationship between $\mathrm{SNR}_{[sym]}$ and SNR for complex input signals, both expressed in dB, is given as

$$\mathrm{SNR}_{[sym]}(\mathrm{dB}) = 10\log_{10}\left[\frac{S.T_{sym}}{N/B_n}\right] = \mathrm{SNR}(\mathrm{dB}) + 10\log_{10}\left(\frac{T_{sym}}{T_{samp}}\right) \qquad \textbf{Eq A.10}$$

where

T_{sym} is the signal's symbol period,

T_{samp} is the signal's sampling period, and

$B_n = 1/T_{samp}$ is the noise bandwidth, in Hz.

For fading channels, the signal-to-noise ratio per bit is expressed as

$$\mathrm{SNR}_{[bit]} = \gamma_b = \frac{E_b}{N_o}\alpha^2 \qquad \textbf{Eq A.11}$$

where α is used to represent amplitude values of the fading channel with respect to E_b/N_o.

A.3 Error Probability (P_e)

The reliability of a digital communication system is commonly expressed in terms of probability of error at the receiver output. If binary data is considered, it is called bit error rate (BER) or probability of bit error. This is basically the ratio between the number of bits in error over the total number of bits transmitted. In case of symbols, it is termed symbol error.

The BER is a function of SNR and is typically a monotonically decreasing function.

For example, in an AWGN channel, the probability of error (symbol error) for rectangular M-ary QAM (e.g. $M = 4$ for16-QAM) modulation can be derived as [28]

$$P_M = 1 - \left[1 - 2\left(1 - \frac{1}{\sqrt{M}}\right) Q\left(\sqrt{\frac{3}{M-1}\frac{E_{av}}{N_o}}\right)\right]^2 \qquad \textbf{Eq A.12}$$

where M is the number of alphabets, E_{av}/N_o is the average $SNR_{[sym]}$ over the M constellation alphabets, $Q(.)$ denotes the Marcum Q function.

In a slow, flat fading environment, the probability of error is obtained by averaging the error in AWGN channel over the fading probability density function as follows [2]:

$$P_e(\Gamma) = \int_0^\infty P_e(\gamma) p(\gamma) d\gamma \qquad \textbf{Eq A.13}$$

where γ represents the SNR of the received signal, $P_e(\gamma)$ is the probability of error for an arbitrary modulation at a specific value of SNR, $p(\gamma)$ is the PDF of SNR due to fading, and Γ is the average value of γ. For instance, in a Rayleigh fading channel, SNR has a chi-square distribution with two degrees of freedom [28].

$$p(\gamma) = \frac{1}{\Gamma} e^{-\frac{\gamma}{\Gamma}} \qquad \textbf{Eq A.14}$$

Using Eq A.14 in Eq A.13, for QPSK modulation in AWGN, the probability of error in a slow, flat fading channel is evaluated as [2]

$$P_{e,QPSK} = \frac{1}{2}\left[1 - \sqrt{\frac{\Gamma}{1+\Gamma}}\right] \qquad \text{Eq A.15}$$

However, to study the effect of frequency-selective fading channel on the probability of error, simulation is considered a major tool.

A.4 DS-CDMA Basics

The DS-CDMA has become a more popular multiple access scheme than other traditional ones, such as Time Division Multiple Access (TDMA) and Frequency Division Multiple Access (FDMA). Figure 30 illustrates how the available bandwidth is shared in each of those techniques [1].

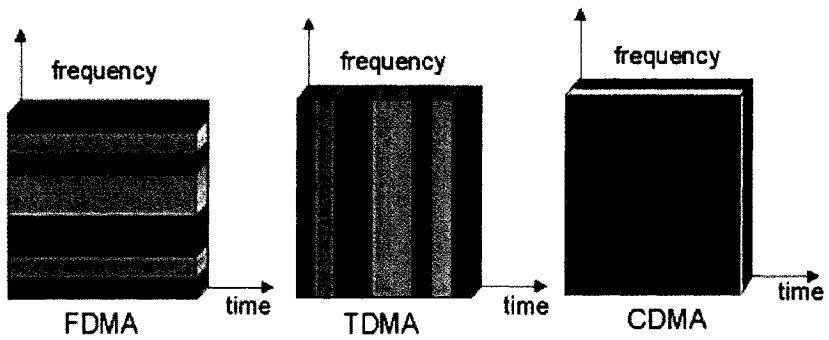

Figure 30: Multiple Access Schemes

In DS-CDMA scheme, spreading (or spread spectrum modulation) is the process of multiplying the narrowband message signal with a larger bandwidth pseudo-noise (PN) sequence (or spreading codes) to produce a wider bandwidth signal. The minimum-duration keying element of the pseudo-noise waveform is called a chip. The spreading operation results in a chip rate that is orders of magnitude greater than the input data bit rate (R_b). In other words, the spread spectrum signals occupy a larger bandwidth (W_{ss}) that is several orders of magnitude greater than the minimum required signal bandwidth ($\sim 1/R_b$). Multiple users can use this larger bandwidth at the same time without

significantly interfering with one another – making spread spectrum systems bandwidth efficient. Figure 31 shows the spreading operation in WCDMA system.

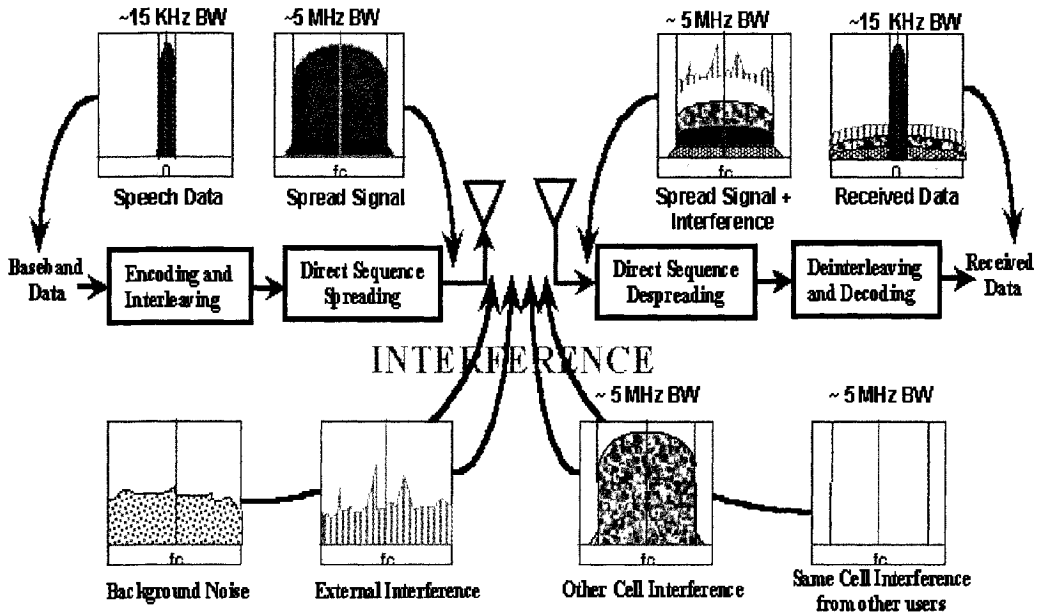

Figure 31: Before and After Spreading in WCDMA [1]

The receiver knows the code-sequence of the user, and it decodes the received signal reliably as the cross-correlation between the codes of the desired user and other users is expected to be very small.

The ratio of the chip rate (R_c) to baseband data bit rate (R_b) is termed Spreading Factor (SF), which is approximately equal to the Processing Gain (PG) due to spreading. Thus,

$$\mathrm{SF} = \frac{R_c}{R_b} \approx \frac{W_{ss}}{W_{bb}} = \mathrm{PG} \qquad \textbf{Eq A.16}$$

where W_{ss} is the spread spectrum bandwidth and W_{bb} is the baseband signal bandwidth.

The higher the SF, the greater the tolerance to intentional interference (jamming) or unintentional interference.

Channel capacity in DS-CDMA is defined as the total number of simultaneous users the system can support, and quality is defined as the perceived condition of a radio link assigned to a particular user. This perceived link quality is directly related to the probability of bit error, or BER.

The number of users that can access the system in single-cell can be derived as

$$N_u = 1 + \frac{W_{ss}/R_b}{E_b/I_o} G_v G_A \qquad \textbf{Eq A.17}$$

where N_u is the number of users, E_b is energy per bit, I_o is total interference and noise power density at the base station, G_v is the voice activity factor, and G_A is the antenna gain factor due to sectorization. From the above equation, it can be claimed that higher SF allows more simultaneous users to access the system, for a given system bandwidth.

The equation, Eq A.17, can be extended to account for interference from other cells in a multi-cell system.

It can be found in the literature that through voice activation and antenna sectorization higher capacity can be achieved in CDMA over TDMA and FDMA [2]. In addition, other merits of CDMA such as coherent transmission and reception, soft-handoff, etc. can assist in increasing channel capacity.

A.5 Mobile Communication Channel

In a mobile communication channel, the received signals undergo (1) large-scale fading (or shadowing) and (2) small-scale fading (or Rayleigh fading) [2]. The former accounts

for slow variations of average signal power attenuation due to motion over large areas. The latter phenomenon accounts for dramatic variation in signal amplitude and phase due to multipath propagation as illustrated in Figure 32.

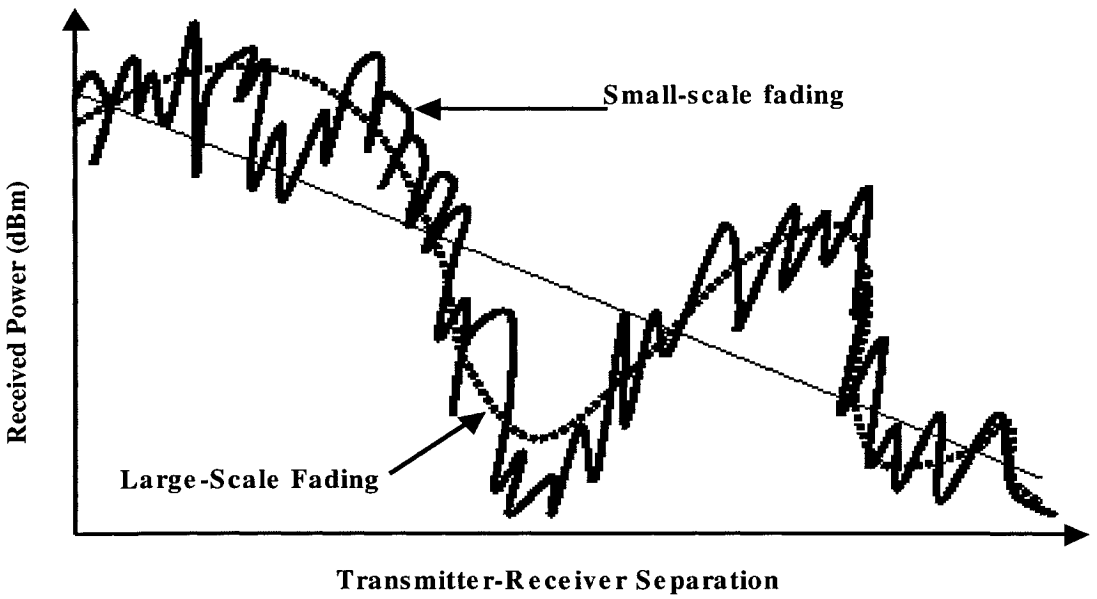

Figure 32: Small-scale and large-scale fading

A.5.1 Multipath Fading (Small Scale Fading)

Multipath propagation occurs when signals arrive at the receiver both directly from the transmitter and via reflections from, or transmission through, an obstacle. Large reflectors, hence long path differences, cause multipath. The amount of signal reflected depends on a number of factors, including the polarization of the incident wave, the angle of arrival, the carrier frequency and the relative permittivity of the surfaces.

While it is a potential problem, multipath also is essential for mobile communications. Without multipath, there would have to be far more base stations to ensure that a direct line of sight existed between the base station and mobile. Multipath effects are more acute in urban built-up areas such as city centers than in rural open countryside. Urban

areas are likely to produce many reflected paths of varying path length. Figure 33 illustrates this phenomenon.

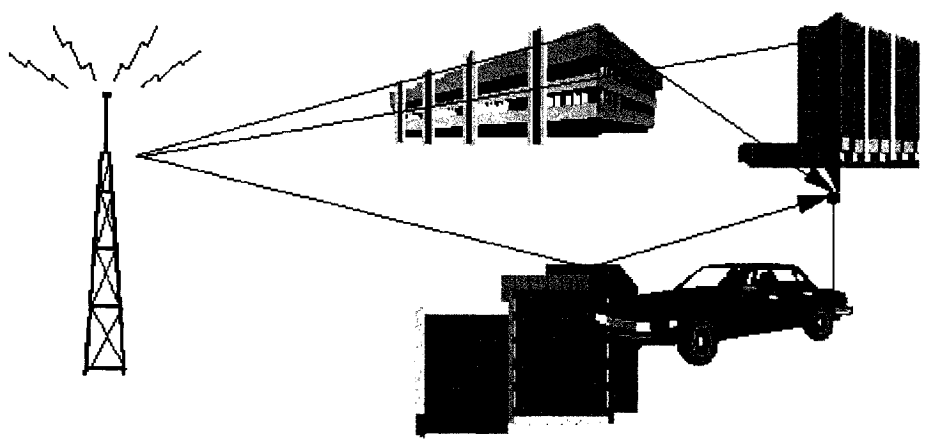

Figure 33: Multipath Due to Scattering

A.5.2 Rayleigh Fading

The multipath fading is commonly modeled as a Rayleigh fading process. Rayleigh fading occurs when a receiver operates in an environment where the received signals are made up of a series of reflections from a number of objects, and there is no significant path between the receiver and the transmitter. In this situation, the signals have traveled via different paths and arrive at slightly different times and with different amplitudes and phases. Hence, the signals can combine constructively or destructively.

The process is modeled as a sum of infinitely many (in practice it is enough with only a few) received reflections from all angles (uniformly) around the receiver. Mathematically, the received signal $r(t)$ can be written as

$$r(t) = g(t) * s(t) \qquad \textbf{Eq A.18}$$

where $s(t)$ is the transmitted signal, $g(t)$ is the impulse response of the channel (or fading process), and * denotes convolution.

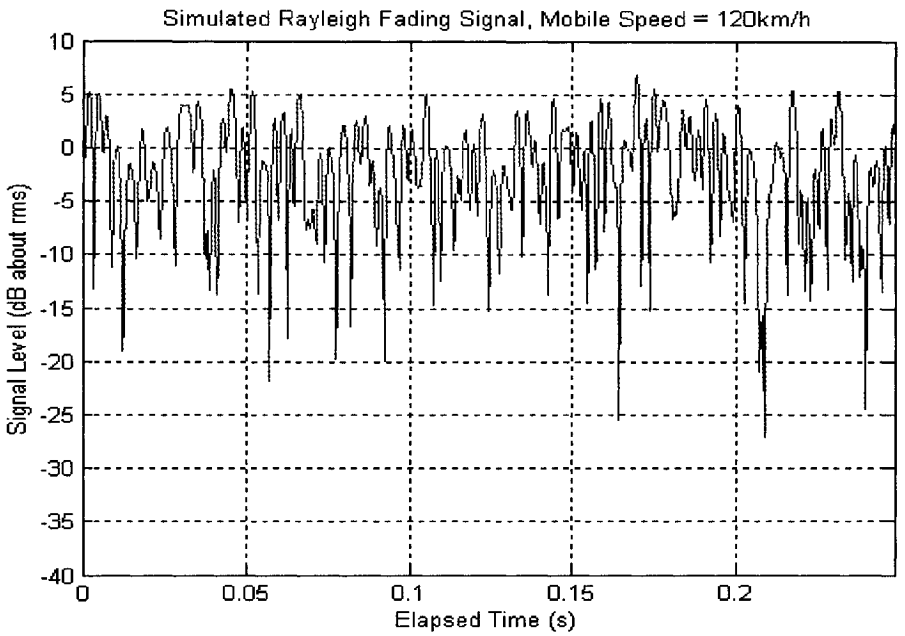

Figure 34: Rayleigh Fading Envelope

The envelope of the received signal has a Rayleigh PDF expressed as

$$p(r) = \begin{cases} \frac{r}{\sigma^2}\exp\left[\frac{-r^2}{2\sigma^2}\right], & 0 \le r \le \infty \\ 0, & r < 0 \end{cases} \qquad \textbf{Eq A.19}$$

where $2\sigma^2$ is the pre-detection mean power of the multipath signal. Figure 34 shows a Rayleigh distributed signal envelope as a function of time. The phase of the Rayleigh fading gain, $g(t)$, is uniformly distributed between 0 and 2π.

A.5.3 Multipath Delay Spread (Time Dispersion)

As demonstrated before, the multipaths signals enroute to a receiver in such a way that the distance traveled and the time the signals arrive will be different for each signal. If this time difference becomes an appreciable percentage of the symbol period, inter-symbol interference (ISI) can occur. This time dispersion of the channel is called multipath delay spread which is an important parameter to access the performance capabilities of wireless systems.

Symbols arriving out of sequence can corrupt preceding or succeeding symbols. The higher the data rate (i.e. WCDMA) or the greater the path-length difference, the more likely it is that delay spread due to multipath will be experienced.

A common measure of multipath delay spread is the root mean square (rms) delay spread (σ_τ). The inverse of the rms delay spread is called coherence bandwidth (B_c). For a reliable communication without using adaptive equalization or other anti-multipath techniques, the bandwidth of the transmitted signal should be much smaller than the coherence bandwidth ($B_s << B_c$).

When the transmitted signal's bandwidth is much smaller than the coherence bandwidth, the wireless channel is referred to as the flat channel or narrowband channel. Flat fading usually causes loss in SNR in the received signal. When the transmitted data rate is closely equal to or larger than the coherence bandwidth, such a channel is called the frequency-selective channel or wideband channel. Frequency selective fading results in channel-induced ISI.

Figure 35 depicts the types of fading based on multipath time delay spread, where B_s is the signal bandwidth and T_s is the symbol period.

Based on Time Dispersion

Flat Fading

1. $B_s < B_c \Leftrightarrow \sigma_\tau < T_s$
2. SNR loss

Frequency Selective Fading

1. $B_s > B_c \Leftrightarrow \sigma_\tau > T_s$
2. ISI
3. Multi-paths resolved

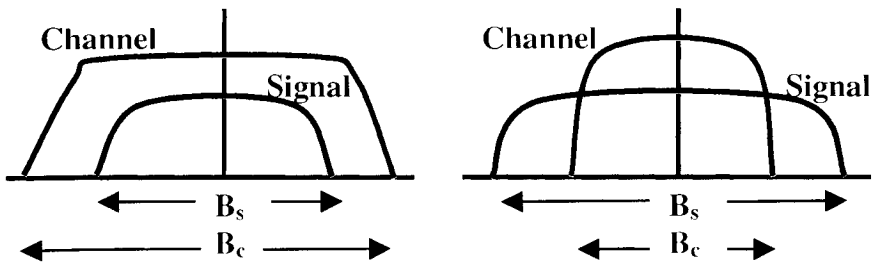

Figure 35: Multipath Fading Channel Characteristics

A.5.3.1 Inter-Symbol Interference and Pulse Shaping

The elongation and smearing of symbols such that the energy from one symbol effects the next ones in such a way that the received signal has a higher probability of being interpreted incorrectly is called Inter Symbol Interference or ISI.

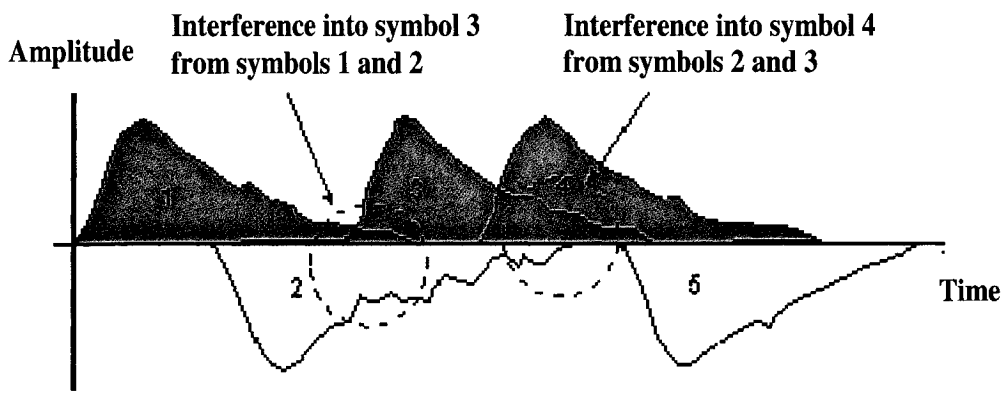

Figure 36: Channel –Induced ISI

One of the phenomena that cause ISI is frequency selective fading in WCDMA systems as mentioned before. Others include filtering effects from hardware, non-linearities and charging effects.

The main tool used to counter ISI is pulse shaping [2], [27]-[28]. The idea of pulse shaping is to keep the symbols interfering in such a way that they do not affect the amplitude at the sampling instant at the receiver. A popular realizable pulse used to shape the transmitted symbols is the so-called Raise Cosine pulse, which satisfies the Nyquist condition for zero-ISI. Thus, the smallest channel bandwidth W for which transmission with zero-ISI is possible is called the Nyquist bandwidth. It is related to the symbol duration T_s as

$$W = \frac{1}{2T_s} \qquad \textbf{Eq A.20}$$

The frequency response of the raised cosine is given by the following formula.

$$H(f) = \begin{cases} 1 & |f| \le \dfrac{(1-\alpha)}{2T_s} \\ \left\{\cos^2 \dfrac{\pi T_s}{2\alpha}\left(|f| - \dfrac{(1-\alpha)}{2T_s}\right)\right\} & \dfrac{(1-\alpha)}{2T_s} \le |f| \le \dfrac{(1+\alpha)}{2T_s} \\ 0 & |f| > \dfrac{(1+\alpha)}{2T_s} \end{cases} \qquad \textbf{Eq A.21}$$

where α is the roll-off factor used to adjust the bandwidth of the pulse between W and $2W$. In effect, the utilized bandwidth W_o of the pulse is

$$W_o = (1+\alpha)R_s \qquad \textbf{Eq A.22}$$

where $R_s = 1/T_s$.

The square root of the frequency response of the raised cosine gives the root-raised cosine in frequency domain. In practice, it has been proven that concatenating two filters each with a root-raised cosine response (called split-filtering) works better. To implement the raised cosine response, the filtering is split in two parts to create a matched set. When the raised cosine filtering is split in two parts, each part is called the root-raised cosine (RRC).

A.5.4 Doppler Shift (Time Variation)

The relative motion between the stationary base station and mobile handset introduces a Doppler frequency shift. This Doppler shift varies with carrier frequency and mobile velocity (with respect to the base station), and affects all multipaths. This determines the speed by which the channel changes. The effect is to introduce another random frequency modulation on top of any Rayleigh fading, thereby compounding an already complicated signal still further.

This movement will cause the channel coefficient, $g(t)$, to be correlated in time (or equivalently in frequency). Different models exist of this correlation but the most common is the classical Jakes model where the correlation function is given as

$$R_g(\tau) = E[g^*(t)g(t+\tau)] = J_0(2\pi f_{\max}\tau) \qquad \textbf{Eq A.23}$$

where $J_0(.)$ denotes the zero-order Bessel function, τ is the sample lag, and f_{max} is the maximum Doppler frequency given by

$$f_{\max} = \frac{v}{c} f_c \qquad \textbf{Eq A.24}$$

where c is the speed of light, f_c is the carrier frequency, and v is the velocity of the mobile. The Doppler fading rate normalized to data rate is called the normalized Doppler frequency and is given as

$$f_{nd} = \frac{f_d}{R_{baud}} = f_d T_s \qquad \textbf{Eq A.25}$$

where f_{nd} is the normalized Doppler frequency, f_d is the physical Doppler frequency, R_{baud} is the symbol rate, and T_s is the symbol period. The normalized Doppler frequency is a measure of the fading rate over many symbols in succession.

The Fourier transform of $R_g(\tau)$

$$S_g(f) = \begin{cases} \dfrac{K}{f_{\max}\sqrt{1-\left(\dfrac{f-f_c}{f_{\max}}\right)^2}} & |f - f_c| < f_{\max} \\ 0 & \textit{otherwise} \end{cases} \qquad \textbf{Eq A.26}$$

is the Classical (Jake's) Doppler spectrum of the complex normally distributed random process $g(t)$. The envelope of $g(t)$, $|g(t)|$, is Rayleigh distributed. Figure 37 shows the power spectrum of the resulting RF signal due to Doppler fading.

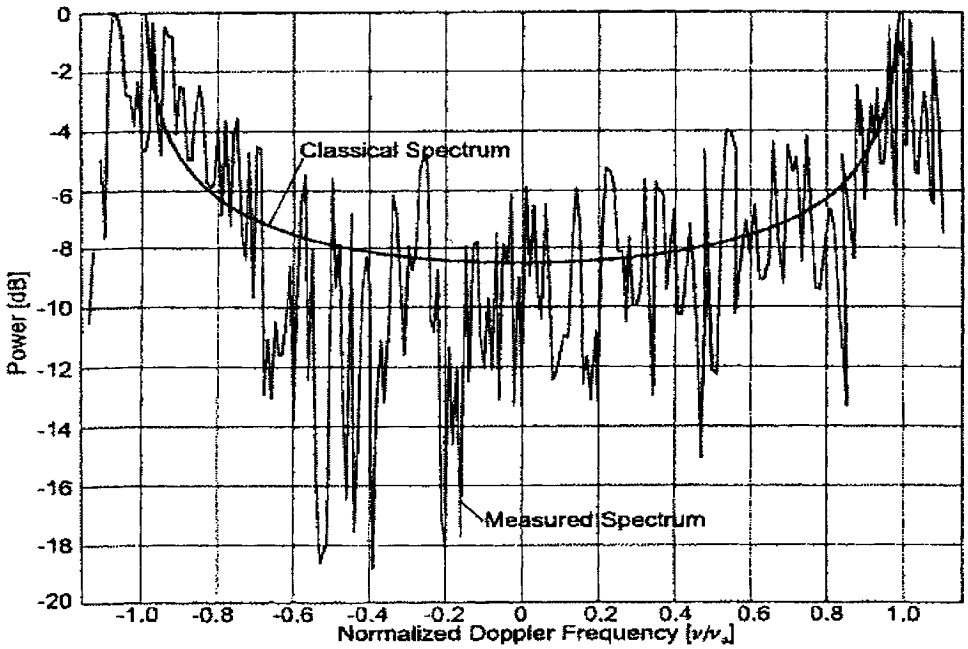

Figure 37: Measured Doppler Spread [29]

A.5.5 Modeling the Fading Channel in Discrete Time

The simulation of Rayleigh fading is best achieved by using an in-phase/quadrature (IQ) modulator driven by two independent and uncorrelated Gaussian noise distributions of equal variance. The 90° phase shift in an IQ modulator ensures that the two noise components are orthogonal. These two Gaussian noise distributions are added to form complex-valued normal random variables.

The Doppler shift component can be simulated, together with Rayleigh fading, by applying sine and cosine waves at the Doppler frequency to the in-phase and quadrature-phase inputs, respectively, in addition to the Gaussian noise.

The multipath Rayleigh fading process is generated using the fading process generators of the form depicted in Figure 38. This IFFT generator is a frequency domain filter

implementation of filter method for generation of a fading process. Parameters that define the generator is the normalized Doppler frequency and the Doppler spectrum.

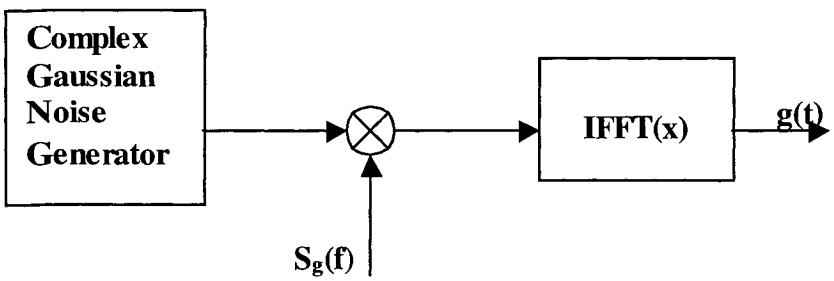

Figure 38: Channel Fading Process

In discrete time, the channel can be modeled as a time variant FIR filter with complex normally distributed tap weights. Thus, the impulse response of the channel is

$$g(t,\tau) = \sum_{l=0}^{L-1} g_l(t)\delta(\tau - \tau_l) \qquad \text{Eq A.27}$$

where L is the number of resolvable multipaths, $g_l(t)$ is the complex-valued channel coefficient for the lth path satisfying the Doppler spectrum equation Eq 1.22, and τ_l is the delay for the lth path. The tap weights for each multipath (i.e. g_1, $g_{2,...}$ g_l) are generated using separate fading process generators of the form in Figure 38. Hence, the impulse response of the channel is modeled as a discrete-time filter or tapped-delay line.

If the channel impulse response is time-invariant (i.e. WSS) over a small-scale time, the above equation can be reduced to

$$g(\tau) = \sum_{l=0}^{L-1} g_l\delta(\tau - \tau_l) \qquad \text{Eq A.28}$$

A.6 Maximum Ratio Combining (MRC) and RAKE Receiver

The signal received at a WCDMA-enabled mobile receiver is the sum of the desired user signal, other users' signals (intra-cell interference) from its own cell, and signals from adjacent cells (inter-cell interference) plus additive white Gaussian noise (AWGN). The task of the receiver is to separate the signal belonging to the user of interest from other interfering signals causing Multiple Access Interference (MAI)

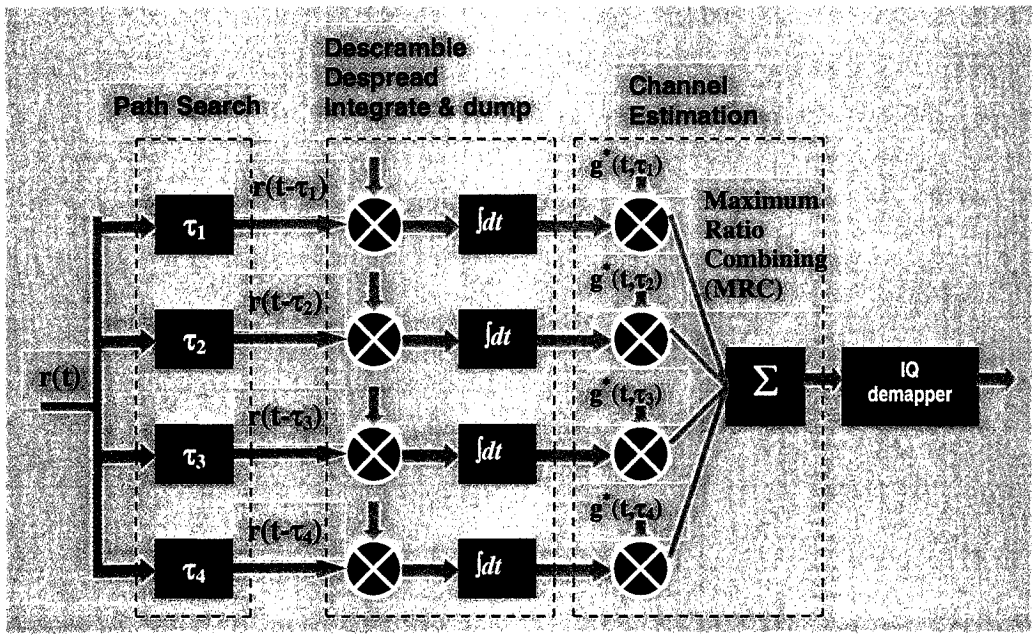

Figure 39: Typical Four-Finger WCDMA RAKE Receiver

In the absence of ISI in an AWGN channel, the optimum way to use signals from multiple paths to decode is Maximum Ratio Combining (MRC) in the sense of highest output SNR (or of the least BER). Traditionally, the so-called RAKE receiver in a mobile handset accomplishes this. The receiver implemented as a bank of matched filters correlates the received signal with the signature chip sequence and maximizes the output signal-to-noise ratio (SNR) by the processing gain, ignoring the existence of multiple access interference (MAI).

When the signals are received with random delays, the cross-correlation between the codes is no longer zero and the signals not of interest contribute to the MAI. When a

large number of interference signals are received with almost identical powers, the MAI appears Gaussian according to the Central Limit Theorem and almost white within the band of interest. Thus, the conventional receiver such as RAKE approaches optimality.

In reality, the MAI is **coloured**; that is, the RAKE finger outputs are correlated. Also, the interference level in each finger is different as the use of orthogonal spreading codes introduces unequal noise powers among fingers (see section 2.3 for properties of OVSF codes) . With these noise properties, the performance requirements for high-speed WCDMA cannot be achieved by using the standard RAKE receiver in downlink.

References

[1] http://www. umtsworld. com/technology/overview. htm: last accessed: September 12, 2005.

[2] T. S. Rappaport, "Wireless Communications – Principles and Practice", Prentice Hall, PTR, New Jersey, July1999.

[3] J. Chen, J. Wang, M. Sawahashi, "MCI Cancellation for Multicode Wideband CDMA Systems", IEEE Journal on Selected Areas in Communications, vol. 20, no. 2, pp. 450-462, February 2002.

[4] G. E. Bottomley, T. Ottosson, Y. -P. E. Wang, "A Generalized RAKE Receiver for Interference Suppression", IEEE Journal on Selected Areas in Communications, vol. 18, no. 8, pp. 1536-1544, August 2000.

[5] G. Kutz and A. Chass, "On the Performance of a Practical Downlink CDMA Generalized RAKE Receiver", Proceedings 56th IEEE VTC, vol. 3, pp. 1352-1356, September 2002.

[6] Y. -P. E. Wang, J. -F. T. Cheng, E. Englund, "The benefits of advanced receivers for high speed data communications in WCDMA", Proceedings 56th IEEE VTC, vol. 1, pp. 132 – 136, September 2002.

[7] H. Hadinejad-Mahram, H. Elders-Boll, G. Alirezai, "Performance Evaluation of Advanced Receivers for WCDMA Downlink Detection", The 5th International Symposium on Wireless Personal Multimedia Communications, vol. 2, pp. 367 – 371, October 2002.

[8] "Services and Service Capabilities", 3GPP TS 22.105, V3.10.0, October 2001.

[9] "High-speed downlink packet access: Physical layer aspects", 3GPP TS 25 .858, V5.0.0, March 2002.

[10] S. Parkwall, E. Englund, P. Malm, T. Hedberg, M. Persson, J. Peisa, " WCDMA evolved – High-speed packet-data services", Ericsson Review, no.2, 2003.

[11] http://products.nortel.com/go/product_content.jsp?segId=0&parId=0&prod_id=52180&locale=en-US : last accessed: September 12, 2005.

[12] T. E. Kolding, F. Frederiksen, P. E. Mogensen, "Performance aspects of WCDMA systems with high speed downlink packet access (HSDPA)", Proceedings 56th IEEE VTC, vol. 1, pp. 477 – 481, September 2002.

[13] "High Speed Downlink Packet Access: Overall UTRAN Description", 3GPP TS 25.855, V5.0.0, August 2001.

[14] J. Wigard, T. Kolding, K. Pedersen, H. Holma, P. Mogensen, "High Speed Downlink Packet Access (HSDPA) for WCDMA", Nokia Networks, November 2003.

[15] "Universal Mobile Telecommunications System (UMTS); Selection Procedures for the Choice of Radio Transmission technologies of the UMTS", TR 101 112 V3.2.0, April 1998.

[16] "Multiplexing and channel coding (FDD)", 3GPP TS 25.212, V6.3.0, December 2004.

[17] "Spreading and Modulation (FDD)", 3GPP TS 25.213, V5.2.0, September 2002.

[18] H. Anton, C. Rorres, "Elementary Linear Algebra - Applications Version", 6th Edition, John Wiley & Sons Inc., 1991.

[19] W. Kahan, "Gauss-Seidel Methods of Solving Large Systems of Linear Equations", Ph.D. Thesis, Toronto, Canada, University of Toronto, 1958.

[20] M. Hestenes, E. Stiefel, "Methods of conjugate gradients for solving linear systems", J. Res. Nat. Bur. Standards 49, pp. 409-436, 1952

[21] C. P. Jackson, and P. C. Robinson, "A Numerical Study of Various Algorithms Related to the Preconditioned Conjugate Gradient Method", Int. J. Num. Meth. Fluids, v. 21, pp. 1315 - 1338, 1985.

[22] S. C. Eisenstat, "Efficient Implementation of a Class of Preconditioned Conjugate Gradient Methods", SIAM J. SCI. STAT. COMPUT., vol. 2, no .1, March 1981.

[23] R. –S. Chen, E. K. –N. Yung, C. H. Chan, D. X. Wang, D. G. Fang, "Application of the SSOR Preconditioned CG Algorithm to the Vector FEM for 3-D Full-Wave Analysis of Electromagnetic-Field Boundary-Value Problems", IEEE Transactions on Microwave Theory and Techniques, vol. 50, no. 4, April 2002.

[24] "User Equipment (UE) radio transmission and reception (FDD)", 3GPP TS 25.101, V6.7.0, March 2005.

[25] J. F. Rossler, J. B. Huber, "Iterative soft decision interference cancellation receivers for DS-CDMA downlink employing 4QAM and 16QAM", Conference Record of the 36th Asilomar Conference on Signals, Systems and Computers, vol. 2, pp. 1488-1494, November 2002.

[26] G. Kutz, A. Chass, "Low Complexity Implementation of a Downlink CDMA Generalized RAKE Receiver", Proceedings 56th IEEE VTC, vol. 3, pp. 1357-1361, September 2002.

[27] S. Haykin, "Communication Systems", 4th Edition, John Wiley & Sons Inc., 2001.

[28] J. G. Proakis, "Digital Communications", 4th Edition, McGraw-Hill, New York, 2001.

[29] http://eeweb. poly. edu/faculty/bertoni/el675. html : last accessed: September 12, 2005.